J. Fluid Mech. (1993), *vol.* 251, *pp.* 533–562

Direct numerical simulation of isotropic turbulence interacting with a weak shock wave

By SANGSAN LEE, SANJIVA K. LELE† AND PARVIZ MOIN‡
Department of Mechanical Engineering, Stanford University, Stanford, CA 94305, USA

(Received 23 July 1992 and in revised form 21 December 1992)

Interaction of isotropic quasi-incompressible turbulence with a weak shock wave was studied by direct numerical simulations. The effects of the fluctuation Mach number M_t of the upstream turbulence and the shock strength M_1^2-1 on the turbulence statistics were investigated. The ranges investigated were $0.0567 \leqslant M_t \leqslant 0.110$ and $1.05 \leqslant M_1 \leqslant 1.20$. A linear analysis of the interaction of isotropic turbulence with a normal shock wave was adopted for comparisons with the simulations.

Both numerical simulations and the linear analysis of the interaction show that turbulence is enhanced during the interaction with a shock wave. Turbulent kinetic energy and transverse vorticity components are amplified, and turbulent lengthscales are decreased. The predictions of the linear analysis compare favourably with simulation results for flows with $M_t^2 < a(M_1^2-1)$ with $a \approx 0.1$, which suggests that the amplification mechanism is primarily linear. Simulations also showed a rapid evolution of turbulent kinetic energy just downstream of the shock, a behaviour not reproduced by the linear analysis. Investigation of the budget of the turbulent kinetic energy transport equation shows that this behaviour can be attributed to the pressure transport term.

Shock waves were found to be distorted by the upstream turbulence, but still had a well-defined shock front for $M_t^2 < a(M_1^2-1)$ with $a \approx 0.1$). In this regime, the statistics of shock front distortions compare favourably with the linear analysis predictions. For flows with $M_t^2 > a(M_1^2-1)$ with $a \approx 0.1$, shock waves no longer had well-defined fronts: shock wave thickness and strength varied widely along the transverse directions. Multiple compression peaks were found along the mean streamlines at locations where the local shock thickness had increased significantly.

1. Introduction

The presence of shock waves is an important feature that distinguishes high-speed supersonic flows. Understanding the mechanisms by which turbulence interacts with a shock wave is of fundamental importance in understanding the complex phenomena of turbulent boundary layer/shock wave interactions. The simplest circumstance in which turbulence interacts with a shock is the case of isotropic turbulence interacting with a normal shock: a problem which is the subject of this paper.

The study of the interaction of turbulence with a shock wave began with the development of linear theories in the early 1950s. Using his general theory of aerodynamic sound generation, Lighthill (1953) estimated the acoustic energy scattered from the interaction of turbulence with a shock wave. Analytical studies of shock–turbulence interaction (Ribner 1953; Moore 1953; Kerrebrock 1956; Chang

† Also with the Department of Aeronautics and Astronautics, Stanford University.
‡ Also with NASA-Ames Research Center.

1957; McKenzie & Westphal 1968) were developed using a linearized description of the interaction of plane disturbances interacting with a shock wave. These disturbances were represented as waves of vorticity, entropy, or sound (Kovásznay 1953). Any one such wave interacting with the shock wave generates all three fluctuations downstream of the shock wave. Ribner (1953) investigated the passage of a single vorticity wave through a plane shock and its modification, with simultaneous generation of a sound wave in a reference frame fixed on the shock wave. This analysis was later extended to study turbulence amplifiation due to a shock wave (Ribner 1954), the flux of acoustic energy emanating from the downstream side of the shock (Ribner 1969), and the one-dimensional power spectra of various fluctuations downstream of the shock (Ribner 1987). Moore (1953) analysed the flow field produced by oblique impingement of weak plane disturbances on a normal shock wave in a reference frame fixed on the mean upstream flow. Anyiwo & Bushnell (1982) revisited the linear analysis to identify primary mechanisms of turbulence enhancement – amplification of the vorticity mode, generation of acoustic and entropy modes from the interaction, and turbulence 'pumping' by shock oscillations.

Debieve, Gouin & Gaviglio (1982) analysed the evolution of turbulence through a shock, and separated the effects of the specific turbulent sources from the effects of the mean motion – convection and production. Their prediction of the longitudinal velocity fluctuation was in good agreement with the experimental results.

Experiments on the interaction of turbulent boundary layers with an oblique shock wave were conducted by Debieve *et al.* (1982), Dolling & Or (1985), Andreopoulos & Muck (1987), and Smits & Muck (1987) amongst others. A general finding from the experiments is that Reynolds shear stress and turbulence intensities are amplified across the shock wave. The interaction of an oblique shock wave with a turbulent boundary layer involves several complex phenomena: (*a*) unsteady flow separation in the interaction region, (*b*) oscillation of the shock wave in the longitudinal direction, (*c*) streamline curvature, and (*d*) inhomogeneity effects due to walls. Because of these complications, it has been difficult to clearly identify through these experiments the sole effect of the shock wave on turbulence.

In order to isolate the effect of a shock wave on turbulence, Debieve & Lacharme (1986) conducted experiments on the interaction between the shock wave and grid-generated turbulence. They measured velocity and temperature spectra upstream and downstream of the shock wave and concluded that turbulent fluctuations are amplified and the Taylor microscales increase during the interaction. An intermittency effect due to unsteady shock wave distortion on turbulence statistics was also clearly described. Keller & Merzkirch (1990) performed an experiment on the interaction of grid-generated turbulence with a shock in a shock tube. They verified amplification of the turbulence intensity quantitatively, showing that amplification was restricted to the lower wavenumbers in the spectrum. Honkan & Andreopoulos (1992) examined the interaction of a normal shock wave with homogeneous grid-generated turbulence. They found that turbulence is considerably amplified during the interaction, and that the amplification factor is not the same at different lengthscales and different turbulence intensities. They also found that large eddies were amplified more than small eddies during the interaction, leading to the increase of a dissipation lengthscale. This was in line with the observation of lengthscale increase made by Debieve *et al.* (1986) and Keller & Merzkirch (1990), but it contradicts the intuitive expectation that mean flow compression should decrease the relevant turbulence lengthscales. As will be shown, these results disagree with the results of the present study. Jacquin, Blin & Geffroy (1991) investigated the interactions of a normal shock wave with grid-

generated turbulence and a turbulent jet, and compared the turbulence amplification with the predictions of linear analysis. They observed that turbulence amplification was not significant for the grid-generated turbulence, and that the decay of turbulent kinetic energy was accelerated downstream of the shock wave.

The aforementioned experiments treated the interaction of a shock with quasi-incompressible turbulence where fluctuations in pressure and density are not significant. An experiment on the interaction of weak shocks ($M_1 = 1.007$, 1.03, and 1.1) with a random medium of density inhomogeneity was performed by Hesselink & Sturtevant (1988). They observed that the pressure histories of the distorted shock waves were both peaked and rounded and explained these features in terms of the focusing/defocusing of the shock front due to inhomogeneity of the medium.

Numerical simulations of the shock–turbulence interaction are just beginning to emerge. Using a shock capturing numerical technique, Rotman (1991) numerically calculated the change in a two-dimensional turbulent flow caused by the passage of a travelling shock wave. He found that the shock causes an increase in the turbulent kinetic energy and that the lengthscale of the turbulent field is reduced upon passage of the shock. He also found that increasing the initial turbulent kinetic energy caused a straight shock wave to evolve into a distorted front. Lee, Lele & Moin (1991*a*) conducted direct numerical simulations of two-dimensional turbulence interacting with a shock wave and found that vorticity amplification compared well with the predictions of the linear analysis, but turbulent kinetic energy evolution behind the shock showed significant nonlinear effects. The energy spectrum was found to be enhanced more at large wavenumbers, leading to an overall lengthscale decrease.

The primary objective of this work is to investigate the interaction of three-dimensional isotropic turbulence with shock waves using direct numerical simulations. Predictions of linear analysis are introduced where distinctions between linear and nonlinear interaction mechanisms are to be made. The numerical and analytical procedures employed in this work are briefly described in §2. In §3, we present the modification of turbulence statistics through the interaction with a shock wave. In §4, the modification of the shock wave structure through the interaction process is described. The summary of our findings is given in §5.

2. Numerical simulation and linear theory

2.1. *Numerical simulation*

The time-dependent Navier–Stokes equations for a compressible fluid were solved directly. In the direct numerical simulation (DNS), all the relevant turbulence scales are resolved without a turbulence model, and the shock wave structure is resolved as a solution of the Navier–Stokes equations without introducing the techniques of shock fitting or shock capturing. The shock structure is adequately represented by the Navier–Stokes equations for Mach numbers less than 2.0 (Sherman 1955). (For polyatomic gases, however, the thickness of the shock wave obtained from a solution of the Navier–Stokes equations is thinner than that of the real shock wave because the rotational energy mode is not in equilibrium inside the shock wave (Lumpkin 1990).)

The governing equations are the continuity equation, three momentum equations, and the energy equation. The corresponding dependent variables are density ρ, three components of momentum ρu_i, and the total energy E_T per unit volume ($E_T = \rho(e + \frac{1}{2}u_i u_i)$, where e is the internal energy), which are made dimensionless by ρ_0, $\rho_0 c_0$, and $\rho_0 c_0^2$, respectively, where ρ_0 and c_0 are the density and the sound speed of a reference state. We assume the fluid to be a perfect gas with constant specific heats, and

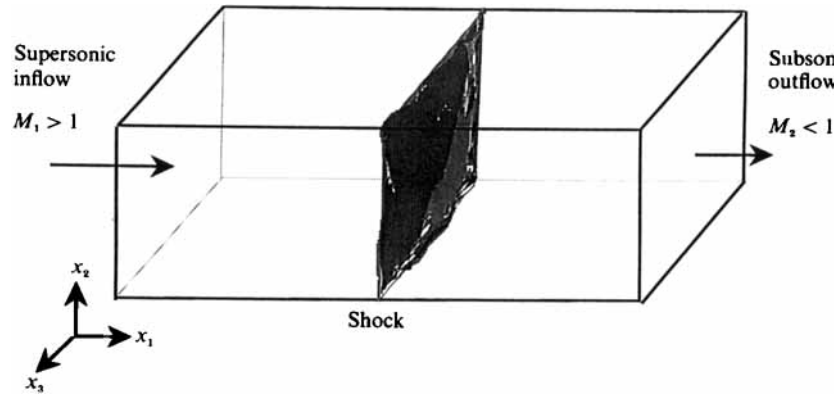

FIGURE 1. Schematic diagram of the computational domain.

the ratio of specific heats, $\gamma = 1.40$. The fluid is assumed to be Newtonian with zero bulk viscosity, and Fourier law is used for the heat flux. The Prandtl number, Pr, is assumed to be constant with a value of 0.75†, and the temperature-dependent viscosity is prescribed with the power law $\mu/\mu_0 = (T/T_0)^n$, where $n = 0.76$.

An explicit time-advancement method is used. The variables $(\rho, \rho u_i, E_T)$ are advanced using a three-step compact-storage third-order Runge–Kutta scheme (Wray 1986). We used the sixth-order compact Padé schemes (Lele 1992*a*) for the approximation of the spatial derivatives. Since the resolution requirements for a shock wave are far more restrictive than those for turbulence, a non-uniform grid is used in the streamwise direction to resolve the shock wave structure.

The schematic diagram of the computational domain is shown in figure 1. The streamwise, or mean shock-normal, direction is chosen to be aligned with the x_1-axis, and turbulence is assumed to be homogeneous in the transverse directions (x_2, x_3), where periodic boundary conditions are applied. The simulations are conducted in a reference frame fixed on the mean shock position so that long-time statistical averages of turbulence quantities can be obtained. In this frame of reference, the mean flow approaches the shock wave with a supersonic speed and leaves with a subsonic speed. Since the upstream flow is supersonic, we can specify all the flow variables at the inflow, while non-reflecting boundary conditions (Thompson 1987) are used at the subsonic outflow boundary. Mean values of velocity, pressure, and density are set to be uniform over the inflow plane. Turbulence generated at the inflow boundary is designed to be isotropic in velocity fluctuations and with no fluctuations in pressure and density. A detailed description and validation of the procedure to generate inflow 'turbulence' with a prescribed spectrum is given in Lee, Lele & Moin (1992*a*). The inflow turbulence has the following three-dimensional energy spectrum function:

$$E(k) = 16\left(\frac{2}{\pi}\right)^{\frac{1}{2}} \frac{u_0^2}{k_0}\left(\frac{k}{k_0}\right)^4 \exp\left[-2\left(\frac{k}{k_0}\right)^2\right], \tag{1}$$

where u_0 is the r.m.s. turbulence intensity and k_0 is the most energetic wavenumber. Subscript zero denotes a reference state, taken as the inflow condition in the simulations.

In a spatially evolving simulation, numerical waves are generated due to spurious

† A laminar shock wave with $Pr = 0.75$ has a special property of constant total enthalpy inside the shock wave, and this Prandtl number is close enough to that of air at standard reference state.

interaction between the inflow and the outflow boundaries (Buell & Huerre 1988). These numerical waves have a wavelength of twice the grid size and propagate from the outflow toward the inflow boundary (Trefethen 1982; Vichnevetsky 1986). To remove these spurious waves, localized filtering near the inflow boundary is used (details may be found in Lee, Moin & Lele 1992*b*).

For a direct numerical simulation of turbulence interacting with a shock wave, spatially evolving turbulence must be properly simulated, the shock wave needs to be well resolved, and the interaction of turbulence with a shock wave must be accurately predicted. A detailed validation of the computer code by separate computations of components of the shock–turbulence interaction problem is reported in Lee *et al.* (1992*b*).

Turbulent fluctuations are defined in terms of the deviation of flow variables from their Favre-averaged values. The following notation is used: $\bar{f}$ is an ensemble average of a flow variable f, and f' is deviation from $\bar{f}$; $\tilde{f}$ is the mass-weighted average of f, and f'' is the fluctuation from $\tilde{f}$ (Favre 1965). That is,

$$f' = f - \bar{f}, \quad \tilde{f} = \overline{\rho f}/\bar{\rho}, \quad f'' = f - \tilde{f}.$$

In the results to follow, it is important to note that near the shock wave, some ensemble-averaged and mass-weighted turbulence statistics are 'contaminated' by the unsteady motion of the shock wave. Thus, the large values of fluctuating quantities are, in most cases, due to oscillation of the shock (Lee *et al.* 1992*b*).

2.2. *Linear theory*

Some aspects of the interaction of turbulence with a shock wave are amenable to linear analysis. For the linear analysis to apply, the upstream Mach number variation must be a small perturbation to the mean upstream Mach number. Furthermore, the time required for turbulence to pass through the shock wave should be small compared to the turbulence timescale, $\bar{\rho}q^2/\epsilon$ ($q^2 = \overline{\rho u_i'' u_i''}/\bar{\rho}$ and $\epsilon = \overline{\tau_{ij}(\partial u_i''/\partial x_j)}$, where τ_{ij} is the viscous stress), so that there would be insufficient time for the redistribution of energy into different scales through nonlinear processes.

In this work, we employed the linear interaction analysis (LIA) of Ribner (1953), where the main interest is the interaction of the upstream vorticity wave with a shock. In LIA, inviscid linear equations for the disturbances are solved downstream of the shock, and the boundary conditions at the downstream side of the shock front are expressed in terms of the upstream disturbances by the use of Rankine–Hugoniot relations. Through LIA, amplitudes, lengthscales, and orientations of downstream refracted or generated waves are represented in terms of those of an upstream vorticity wave.

Since fluctuations in weak compressible turbulence can be regarded as a sum of vorticity, entropy, and acoustic waves, the modification of turbulence through the interaction can be predicted via LIA (Ribner 1954, 1969, 1987). In this work, the LIA procedure is revisited to predict modifications of turbulence and the shock wave. Modifications of some turbulence statistics previously reported by Ribner (1954, 1987) are reproduced in the present paper for completeness.

3. Modification of turbulence

The parameters of the simulations are the upstream mean Mach number M_1, fluctuation Mach number $M_t = q/\bar{c}$, and turbulent Reynolds number Re_T. Resolution of the shock wave structure limits the range of shock wave strengths; mean upstream

Case	A	B	C	D	E	F
Grid	129×64^2	129×64^2	193×64^2	129×64^2	129×64^2	129×64^2
M_1	1.20	1.20	1.20	1.20	1.10	1.05
M_t	0.110	0.102	0.0953	0.0567	0.0762	0.100
Re_T	238	133	84.7	170	281	179
Re_λ	19.9	14.9	11.9	16.8	21.6	17.3
k_0	4	5	6	4	4	6

TABLE 1. Parameters for the simulations of shock-turbulence interaction. $Re_\lambda = \bar{\rho} u_{\rm rms} \lambda_1/\bar{\mu}$, where λ_1 is defined in equation (2), and k_0 is defined in equation (1).

Mach number in the range $1.05 \leqslant M_1 \leqslant 1.20$ was used in the present work. Upstream of the shock wave turbulence is isotropic with $M_t < 0.2$, and compressibility effects are negligible (Lee, Lele & Moin 1991*b*). The range of M_t studied in this work was $0.057 \leqslant M_t \leqslant 0.110$. The resolution requirement of turbulence lengthscales limits the range of Reynolds numbers. Here we define a turbulent Reynolds number,

$$Re_T = \frac{(\overline{\rho u_i'' u_i''})^2}{\bar{\mu}\bar{\epsilon}}.$$

The Reynolds number range in the simulation was $80 \leqslant Re_T \leqslant 300$.

This paper is limited to the study of the interaction between weak shock waves and weakly compressible isotropic turbulence at low turbulent Reynolds numbers. Table 1 lists the simulation parameters, where the values of M_t and Re_T are taken at the location immediately upstream of the shock wave.

3.1. *Upstream turbulence*

Since the inflow 'turbulence' is artificial, the flow takes some distance to evolve into a realistic turbulent flow. For all the cases listed in table 1, the computational box upstream of the shock was sufficiently long so that the turbulence interacting with the shock wave was a realistic field of isotropic turbulence with the velocity-derivative skewness, $\overline{u'^3_{1,1}}/(\overline{u'^2_{1,1}})^{\frac{3}{2}}$, ranging between -0.4 and -0.5 (Tavoularis, Bennett & Corrsin 1978). The two-point correlations of fluctuations in velocities, density, and pressure are shown in figure 2(*a*) for case A. The longitudinal velocity correlation $Q_{22}(r_2)$ decays monotonically to zero as expected. The lateral velocity correlations, $Q_{11}(r_2)$ and $Q_{33}(r_2)$, show approximate isotropy. The correlations of pressure and density fluctuations are found to be nearly identical. Figure 2(*b*) shows the one-dimensional power spectra of velocity components and density upstream of the shock wave for case C (this case has the largest k_0/k_c, where k_c is the largest wavenumber represented in the simulation). The Kolmogorov wave number $k_\eta = (\epsilon/\bar{\rho}\bar{\nu}^3)^{\frac{1}{4}}$ of this simulation was $k_\eta/k_0 = 4.63$, or $k_\eta/k_c = 0.869$ at the inflow. The laminar shock wave thickness, δ_s^L (the superscipt L denotes the laminar state), defined as

$$\delta_s^L = \frac{\Delta U_1^L}{|{\rm d}U_1^L/{\rm d}x_1|_{\max}},$$

is comparable to the Kolmogorov lengthscale, $\eta_K = 1/k_\eta$ ($\eta_K/\delta_s^L = 0.96$ in case C), and the Taylor microscale, λ_α, defined as

$$\lambda_\alpha = (\overline{u'^2_\alpha})^{\frac{1}{2}}/(\overline{u'^2_{\alpha,\alpha}})^{\frac{1}{2}}, \tag{2}$$

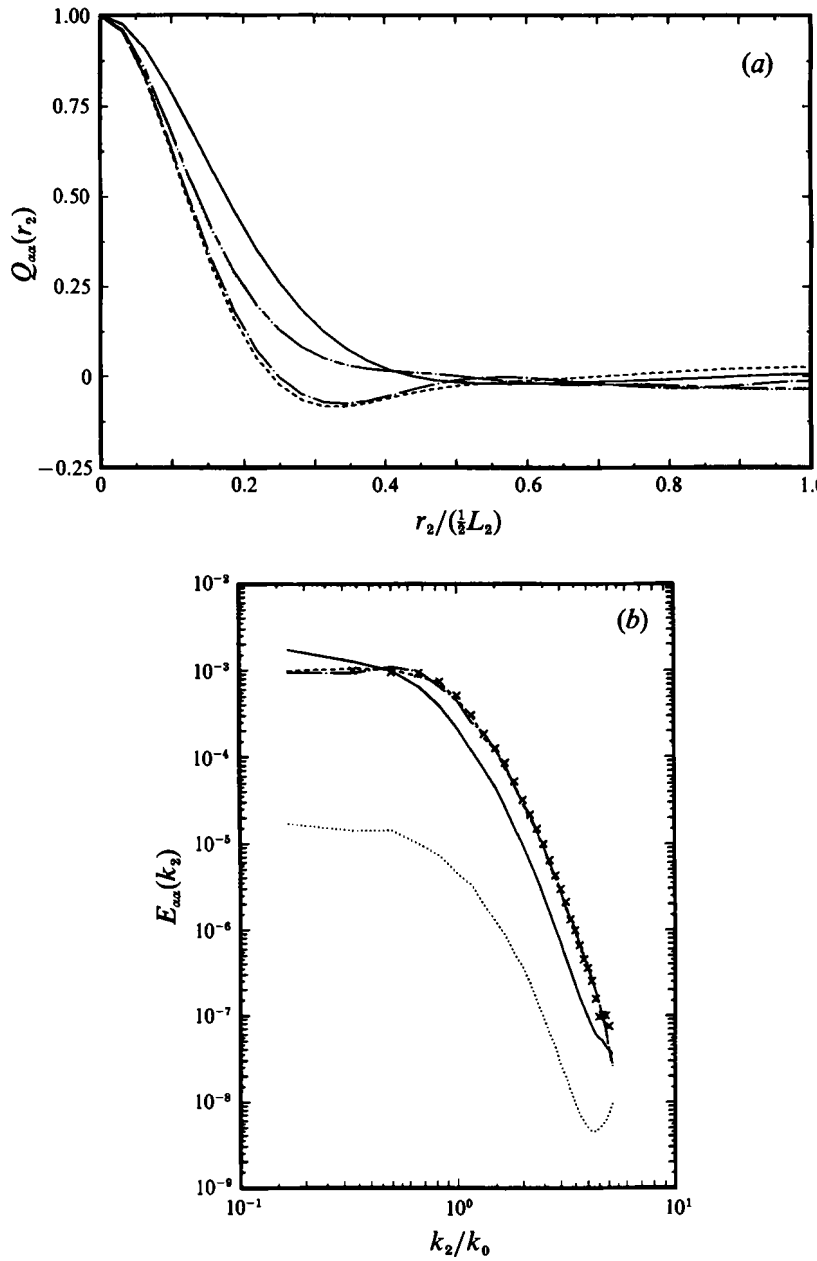

FIGURE 2. (*a*) Two point correlations upstream of the shock wave ($k_0 x_1 = 9.07$) for case A, where the mean shock position $k_0 x_1 = 12.6$; ——, Q_{22}; – – – –, Q_{11}, —·—, Q_{33}; · · · · · ·, $Q_{\rho\rho}$; ——, Q_{pp}. (*b*) One-dimensional power spectra upstream of the shock wave for case C at $k_0 x_1 = 15.8$ ($k_0 x_1^s = 18.8$): ——, E_{22}; – – – –, E_{11}; —·—, E_{33}; · · · · · ·, $E_{\rho\rho}$; ×, E_{11} from E_{22} using the isotropy relation.

is an order of magnitude larger than the shock wave thickness ($\lambda_1/\delta_s^L = 8.9$ in case C). The velocity spectra decay at least five orders of magnitude. Thus, in the worst scenario unresolved turbulence energy is estimated to be less than 0.01 % of the resolved energy, which implies that the simulation represents all the important turbulence energetics. Despite a slight pile-up at high wavenumbers, the density spectrum decays at least three decades. The spectra of $E_{11}(k_2)$ and $E_{33}(k_2)$ are in good agreement, as expected for

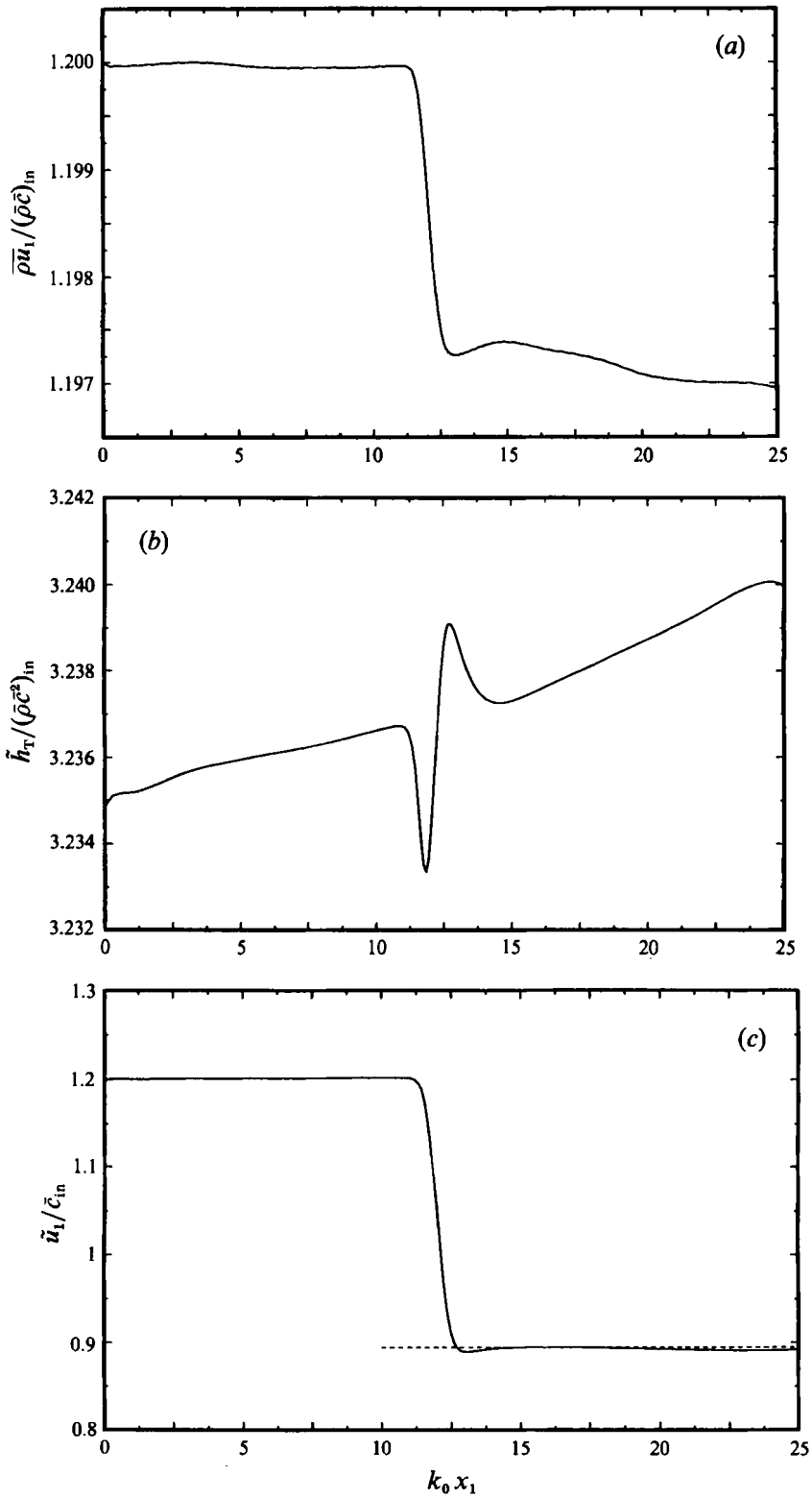

FIGURE 3(*a–c*). For caption see facing page.

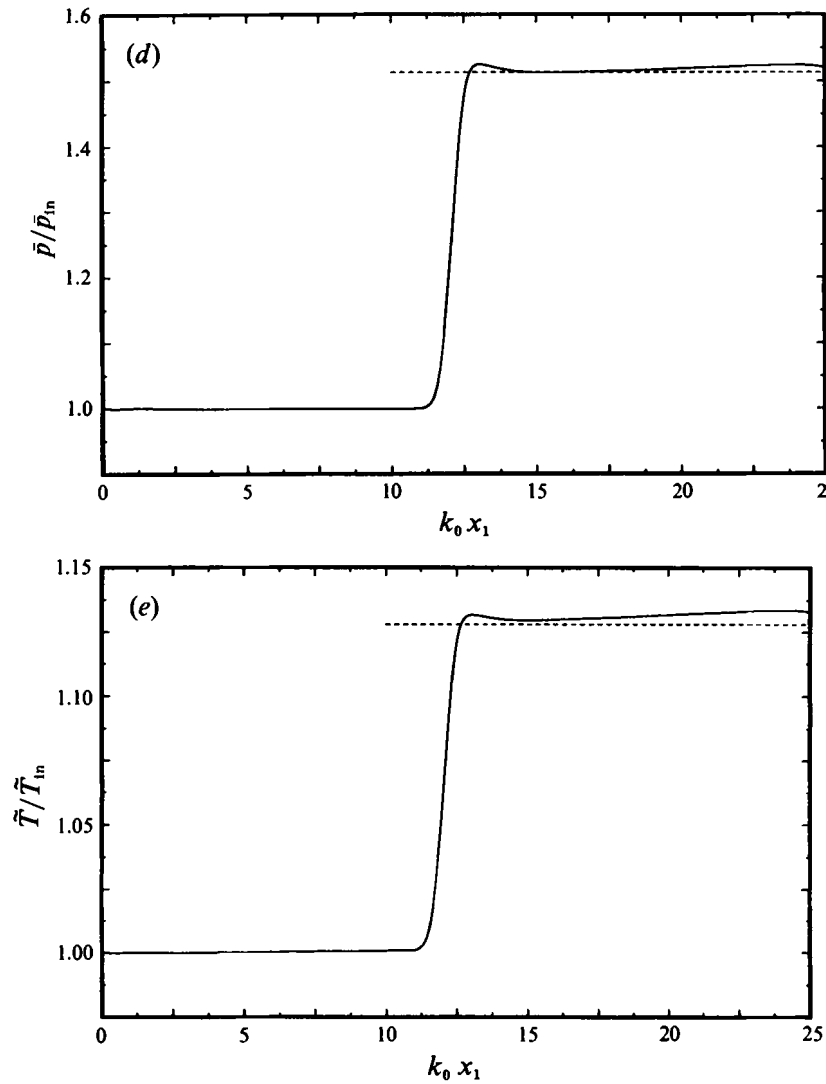

FIGURE 3. Evolution of mean quantities across the shock wave for case A: (*a*) mass flux, (*b*) total enthalpy, (*c*) streamwise velocity, (*d*) pressure, (*e*) temperature. Dashed lines in (*c–e*) denote the laminar downstream values.

isotropic turbulence. The relation between the spectra $E_{11}(k_2)$ and $E_{22}(k_2)$ for isotropic turbulence,

$$E_{11}(k_2) = \frac{1}{2}\left[E_{22}(k_2) - k_2 \frac{\partial E_{22}(k_2)}{\partial k_2}\right]$$

(Hinze 1975) is also satisfied.

3.2. *Mean flow variables*

Figure 3(*a–e*) shows the evolution of mean flow quantities across the shock wave for case A. Mass flux in a coordinate system fixed on the mean shock position is constant throughout the flow field. The average mass flux drops slightly (0.3 %) across the shock wave, which causes a very slow drift of the mean shock position. This reflects the fact

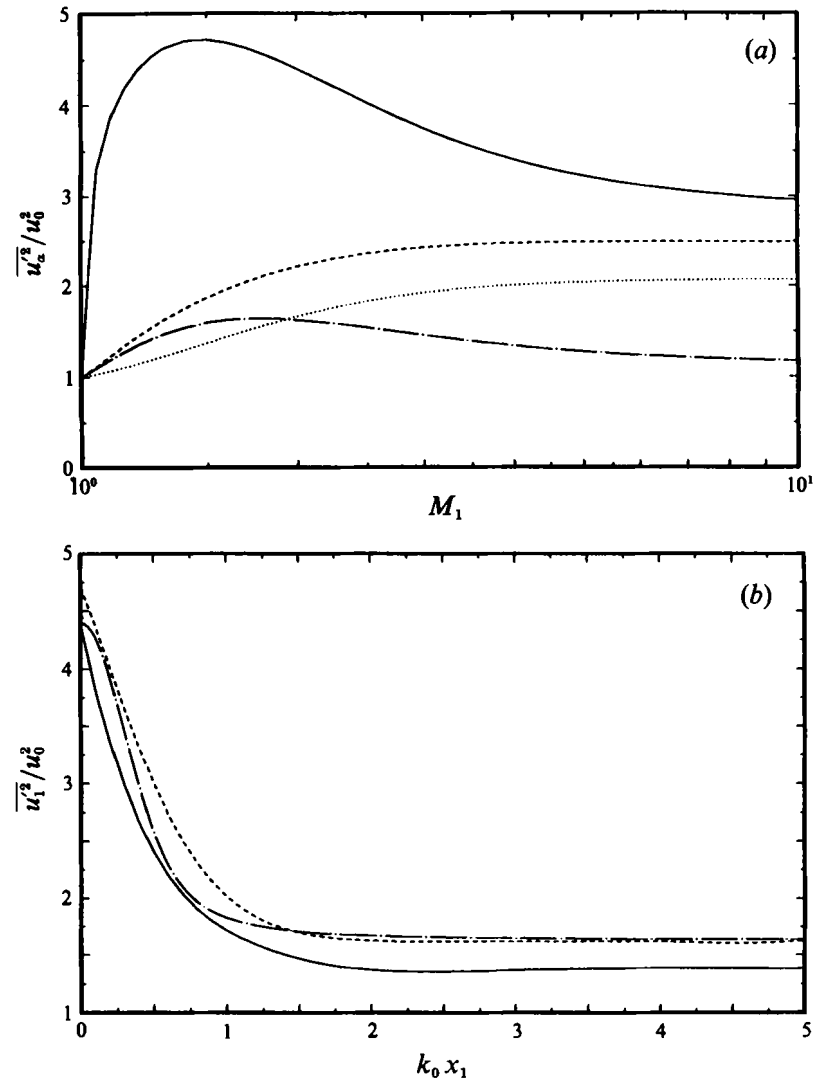

FIGURE 4. (*a*) LIA predictions of velocity component amplifications in the near field and far field: ——, u_1' (near); – – – –, u_2' and u_3' (near); —·—, u_1' (far); · · · · · ·, u_2' and u_3' (far). (*b*) Decay of streamwise velocity fluctuation behind the shock wave: ——, $M_1 = 1.2$; – – – –, $M_1 = 1.5$; —·—, $M_1 = 2.0$.

that the mean turbulent shock propagation speed is different from the specified laminar shock propagation speed (Lele 1992*b*). In the case shown, the mean shock position drifts toward the inflow, and the drift speed is estimated to be about 0.7% of the average upstream flow speed.

Total enthalpy, $h_T = c_p T + \frac{1}{2} u_i u_i$, is conserved across the shock wave and constant inside the shock wave for laminar flows with $Pr = 0.75$ in the coordinate system fixed on the shock wave. In the turbulent case, the mean total enthalpy increases slightly both upstream and downstream of the shock wave, and undergoes a rapid change inside the shock wave. The change inside the shock wave is less than 0.2% of the average total enthalpy. For turbulent flows in a shock-free region, the quantity,

$$\bar{\rho}(\tilde{u}_1 \tilde{h}_T + c_p \widetilde{T'' u_1''} + \tilde{u}_1 \widetilde{u_1'' u_1''} + \tfrac{1}{2} \widetilde{u_k'' u_k'' u_1''}) + \overline{u_k'' \tau_{1k}}$$

is conserved rather than $\tilde{h}_T$. The increase of $\tilde{h}_T$ in the shock-free regions is mainly balanced by the change of the streamwise velocity fluctuation, and $\tilde{h}_T + \widetilde{u_1'' u_1''}$ stays fairly constant.

The mean streamwise velocity, pressure and temperature undergo rapid jumps through the shock wave. The downstream pressure and temperature values are slightly higher than those for the corresponding laminar shock wave. The mean temperature rises slightly (by less than 0.4% of the mean temperature level) downstream of the shock wave. The temperature rise is caused, in part, by the irreversible energy transfer from turbulent kinetic energy to the internal energy by viscous dissipation. Downstream of the shock wave, work done by the mean pressure gradient is comparable to the viscous dissipation, and the combined effects are responsible for more than 98% of the temperature rise. Mean pressure and temperature undergo slight overshoots just behind the shock wave, followed by a relaxation due to non-equipartition of energy between fluctuations in compressible pressure and dilatational velocity through the shock wave (Coleman & Mansour 1991; Sarkar *et al.* 1991). Even though the magnitude of the overshoot is small compared to the jump across the shock wave, it contributes substantially to the level of the velocity fluctuation.

3.3. *Turbulent kinetic energy*

Interaction of vortical waves with a shock wave generates acoustic waves downstream of the shock, parts of which undergo rapid inviscid decay (for more details, see Ribner 1953). Figure 4(*a*) shows the near-field and far-field velocity fluctuations for various shock strengths obtained using LIA. All components of the fluctuating velocities are amplified through the interaction. The decaying acoustic waves contribute significantly to the streamwise velocity fluctuations just behind the shock. The streamwise velocity fluctuations are larger than the transverse velocity fluctuations far away from the shock for $M_1 < 2.0$, which includes the entire range of the present simulations. Figure 4(*b*) shows the decay of the streamwise velocity fluctuations for upstream turbulence with spectrum (1) predicted by the linear analysis. The fluctuations decay monotonically over short distances behind the shock wave ($k_0 x_1 < 1.5$). Transverse velocity fluctuations also undergo monotonic decays over about the same distances behind the shock.

Figure 5 shows the evolution of the diagonal components of the Reynolds stress tensor R_{ij} in the numerical simulation for case C, where R_{ij} is defined by

$$R_{ij} = \widetilde{u_i'' u_j''} = \overline{\rho u_i'' u_j''}/\bar{\rho}.$$

The off-diagonal components of R_{ij} stay close to zero over the entire flow field since turbulence is isotropic upstream and axisymmetric downstream of the shock. The streamwise component in the shock zone contains intermittency effects due to the oscillations of the shock (for more details of the intermittency effects, see Lee *et al.* 1992*b*). The boundaries of the shock oscillations are defined as the locations where $\mathrm{d}\bar{u}_1/\mathrm{d}x_1 = 0$; $\mathrm{d}\bar{u}_1/\mathrm{d}x_1$ is negative only inside the shock wave and slightly positive elsewhere due to viscous heating. All the velocity fluctuations are enhanced during the interaction. The velocity fluctuations are axisymmetric behind the shock wave. Their return to isotropy is found to be negligible compared to the decay. The amplification in the transverse velocity fluctuation variance, which is defined as the ratio of the downstream maximum value to the upstream minimum value, lies between the near-field and far-field predictions of LIA. The streamwise component R_{11} undergoes a rapid increase behind the shock wave, while LIA predicts a monotonic decay for all the velocity fluctuations (figure 4*b*).

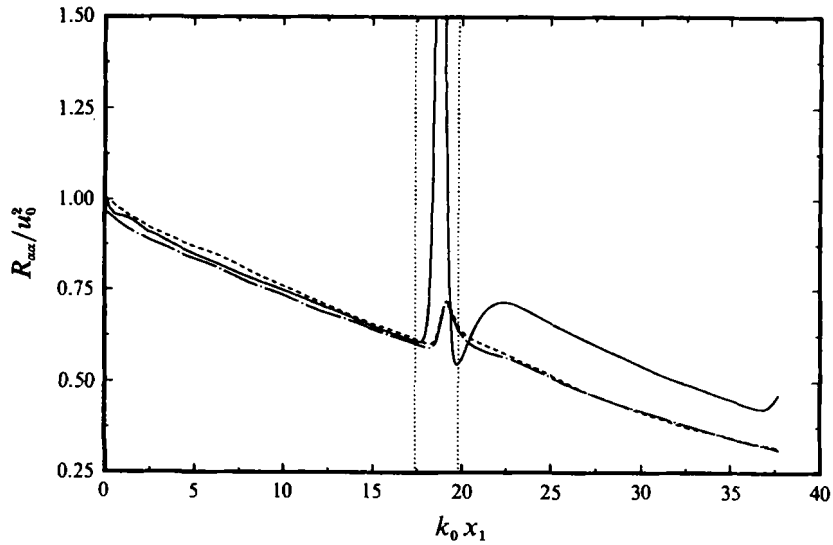

FIGURE 5. Evolution of the normal components of the Reynolds stress for case C: ——, R_{11}; – – – –, R_{22}; —·—, R_{33}. Vertical lines denote the boundaries of shock intermittency.

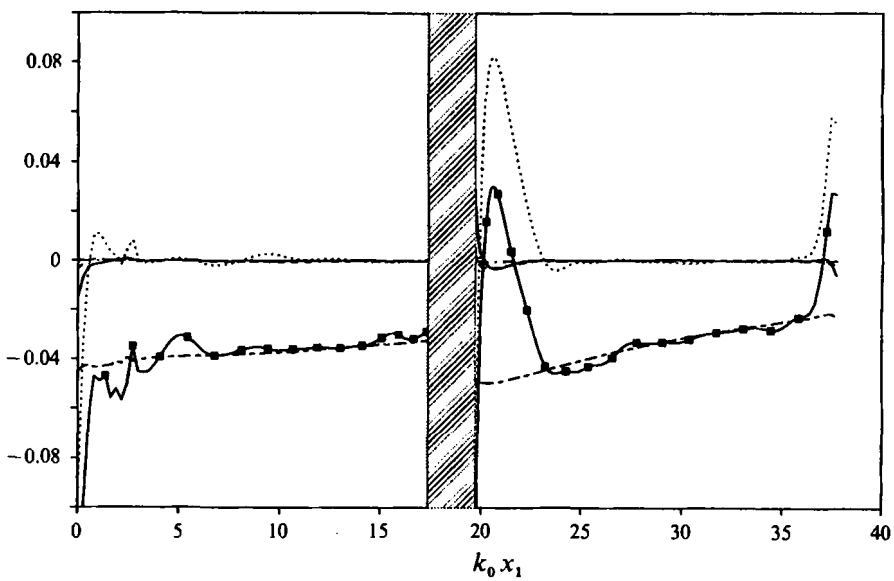

FIGURE 6. Budget of terms in TKE transport equation scaled with $\rho_0 c_0 u_0^2 k_0$ for case C: —■— convection (I); – – – –, production by the mean strain (II); —·—, production by mass flux fluctuation (III); ·····, pressure work (IV); ——, turbulent transport (V); – – – –, viscous term (VI). The shaded region is where turbulence statistics are affected by the shock intermittency.

In order to identify the mechanisms of amplification and rapid evolution of turbulent kinetic energy (TKE), the terms in the transport equation of TKE (Favre *et al.* 1976) were computed. Only the TKE budget is discussed in detail here. Details of the R_{ij} budget may be found in Lee *et al.* (1992*b*). The TKE transport equation is

$$\underbrace{\bar{\rho}\tilde{u}_k \frac{\partial q^2/2}{\partial x_k}}_{\text{(I)}} = \underbrace{-\bar{\rho} R_{ik} \frac{\partial \tilde{u}_i}{\partial x_k}}_{\text{(II)}} \underbrace{-\overline{u_i''} \frac{\partial \bar{p}}{\partial x_i}}_{\text{(III)}} \underbrace{-\overline{u_i'' \frac{\partial p'}{\partial x_i}}}_{\text{(IV)}} \underbrace{-\frac{\partial \overline{\rho u_i'' u_i'' u_k''/2}}{\partial x_k}}_{\text{(V)}} + \underbrace{\overline{u_i'' \frac{\partial \tau_{ik}}{\partial x_k}}}_{\text{(VI)}}. \tag{3}$$

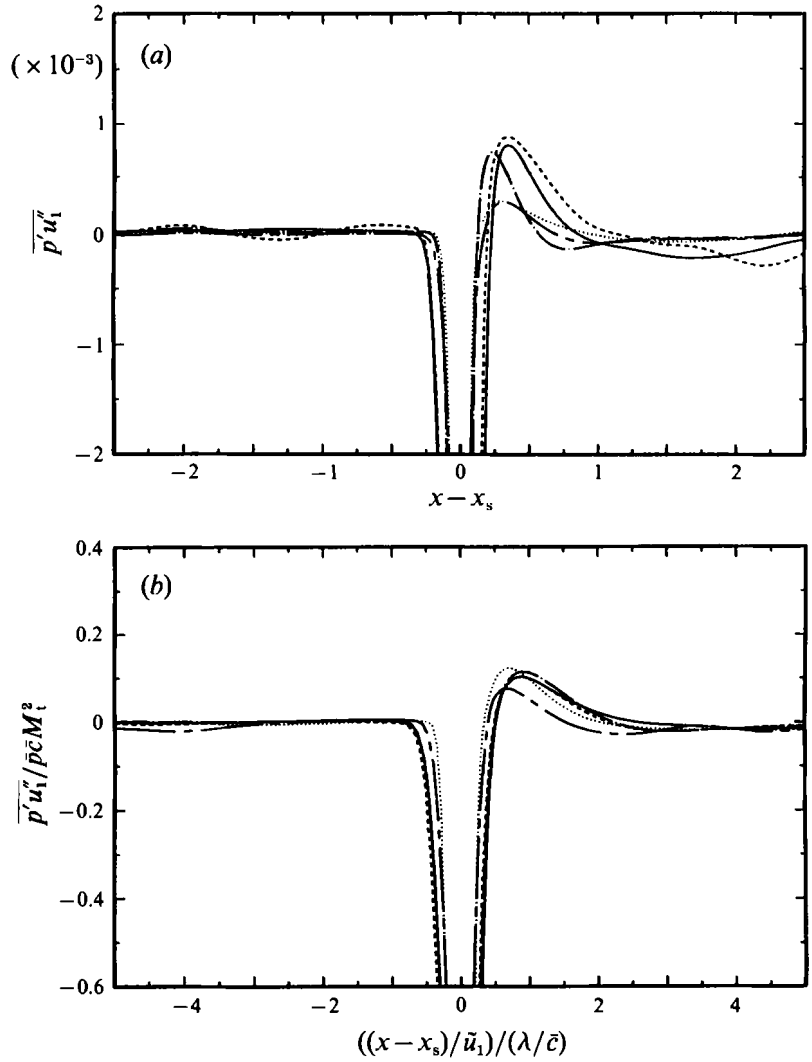

FIGURE 7. (*a*) Unscaled and (*b*) scaled pressure–velocity correlations (x_s is the position for the peak negative correlation): ——, case A; – – – –, case B; —·—, case C; · · · · · ·, case D; ——— , case E.

The convection of TKE (I) is equal to the sum of production by the mean strain field (II) and that by the mass fluctuation (III), the pressure work (IV), the turbulent transport (V), and the viscous dissipation and transport (VI).

Figure 6 shows the budget. The statistics of the flow variables inside the shock wave are contaminated by the intermittency effect caused by the unsteady distortion of the shock wave (Lee *et al.* 1992*b*). Mechanisms of velocity fluctuation amplification in shock–turbulence interaction cannot, therefore, be unambiguously identified by investigating turbulence statistics inside the shock zone. Outside the shock wave, the viscous dissipation is the dominant term and the pressure work is the only other term that has a comparable magnitude. The rapid evolution of TKE just downstream of the shock wave (figure 5) is caused by this pressure work. The pressure work term can be decomposed into two physically distinct terms: the pressure–dilatation $\overline{p'u_{i,i}''}$ and the pressure transport term $(\overline{p'u_i''})_{,i}$

$$-\overline{p'_{,i}u_i''} = \overline{p'u_{i,i}''} - (\overline{p'u_i''})_{,i}.$$

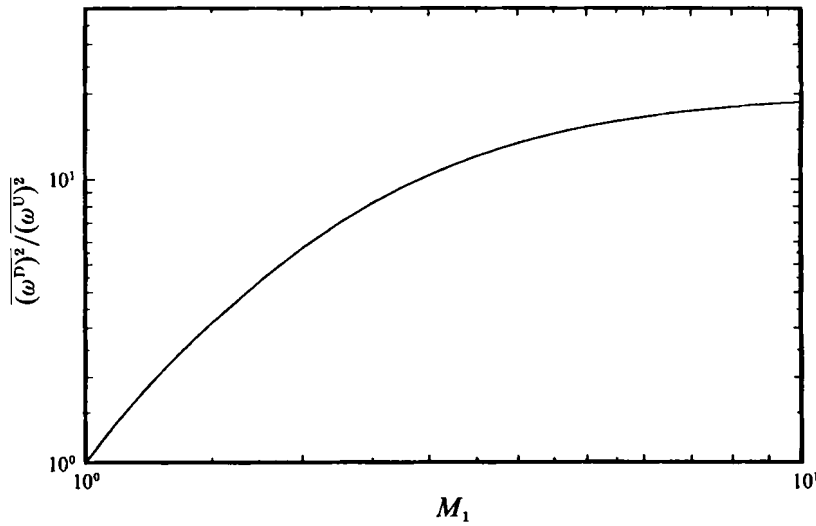

FIGURE 8. LIA prediction of transverse vorticity amplification. The superscripts U and D denote the upstream and downstream states respectively.

A positive pressure–dilatation leads to a reversible energy transfer from the mean internal energy to the TKE, while pressure transport contributes to a redistribution of TKE in the inhomogeneous direction. The decomposition downstream of the shock wave shows that the pressure transport is the main contributor to the pressure work term, thus the rapid evolution of TKE is caused by the pressure transport term, and pressure–dilatation acts mainly to convert the mean internal energy into turbulent kinetic energy, leading to the relaxation from the mean temperature overshoot downstream of the shock wave (figure 3*e*).

To gain insight into the physics of the pressure transport downstream of the shock, several different scalings of $\overline{p'u_1''}$ were examined. The best scaling for collapsing the $\overline{p'u_1''}$ evolution of cases A–E is based on the assumption that the correlation between the pressure and velocity fluctuations is mainly from the acoustic waves. The correlation and the streamwise distance are scaled as

$$\frac{\overline{p'u_1''}}{\bar{\rho}\bar{c}M_t^2} \quad \text{and} \quad \frac{x_1/\tilde{u}_1}{\lambda/\bar{c}},$$

respectively, where λ is a Taylor microscale. The unscaled and scaled results are shown in figures 7(*a*) and 7(*b*), respectively. The scatter in the unscaled case is as much as a factor of five, which is reduced to less than 30% in the scaled case. This suggests that the rapid evolution of TKE may be caused by the propagation of acoustic waves generated during the interaction.

Use of a non-reflecting boundary condition (Thompson 1987) at the outflow generated the anomalous behaviour near the outflow boundaries seen in figures 6, 7(*a*) and 7(*b*). This is due to an incomplete suppression of the acoustic wave reflection. To check that this anomalous behaviour does not contaminate the overall evolution of the flow downstream of the shock wave, the more refined boundary condition of Giles (1990) was implemented in the code. These numerical experiments verified that the undesirable behaviour was indeed confined to only a small region near the outflow boundary and the statistics over the rest of the domain remain unaltered (for more details, see Lee *et al.* 1992*b*).

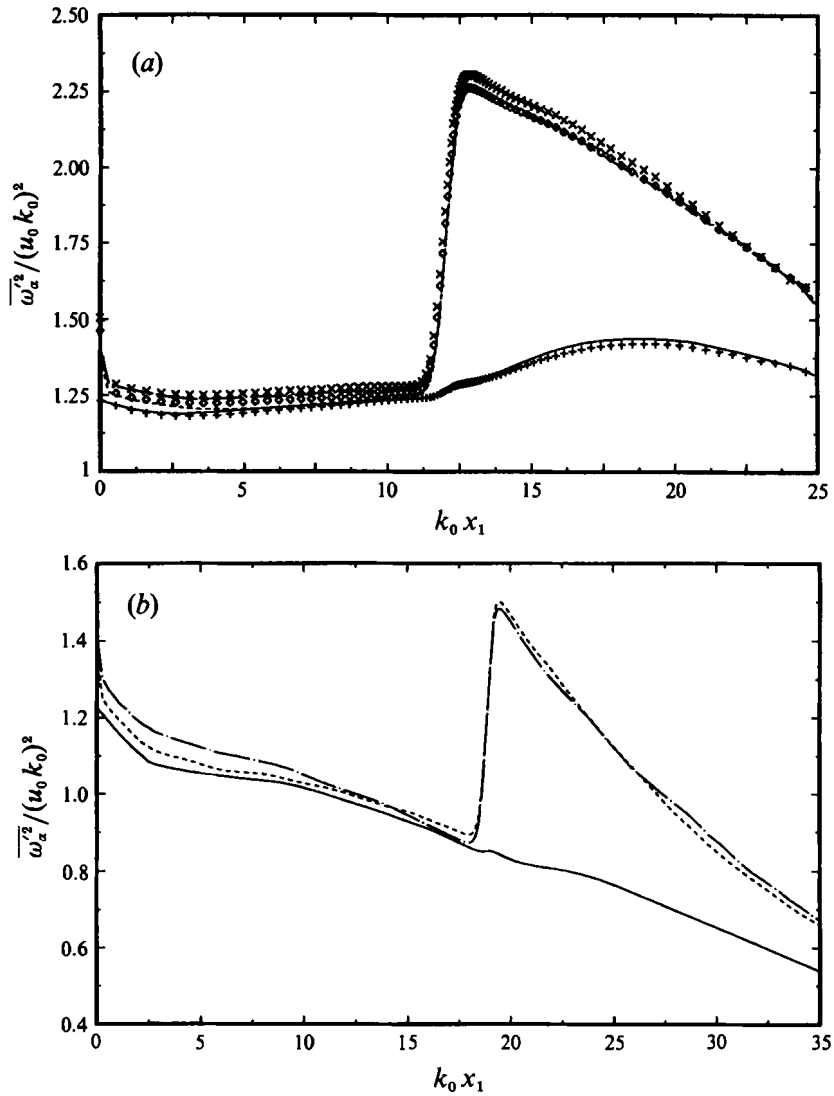

FIGURE 9. Evolution of components of vorticity for (*a*) case A ($Re_T = 240$) and (*b*) case C ($Re_T = 84.8$): ——, ω_1; – – –, ω_2; —·—, ω_3. Symbols in (*a*) are from the simulation with $97 \times 48 \times 48$ grid points: +, ω_1; ×, ω_2; ◇, ω_3.

3.4. *Vorticity*

Variance of vorticity fluctuation is a main contributor to the TKE dissipation rate. Figure 8 shows the prediction of LIA for the amplification of transverse vorticity components across the shock wave. LIA predicts that the streamwise component remains unchanged. As the strength of the shock wave increases (higher mean Mach number), the ratio of the downstream to upstream vorticity also increases. The asymptotic value of the amplification factor for the mean-square transverse vorticity components is about 20 for a shock wave with very large Mach number.

Figures 9(*a*) and 9(*b*) show the evolution of vorticity components in numerical simulations for cases A and C, respectively. As expected the transverse components are amplified across the shock, while the streamwise component is hardly affected: turbulence behind the shock wave becomes axisymmetric in vorticity fluctuations as

well as in velocity fluctuations. Vorticity amplification is consistent with the experimental observation by Jacquin *et al.* (1991) of an increased TKE dissipation rate behind the shock wave. The amplification ratios of the transverse vorticity across the shock wave computed from the simulations compare favourably with the LIA predictions: the maximum difference is about 5% for case F with $M_1 = 1.05$ and $M_t = 0.10$, where the local shock wave structure is significantly modified (see figure 14). Even though amplifications of transverse components of vorticity are very close to the LIA predictions, they are systematically lower. Moveover, the difference becomes larger for higher upstream turbulence levels, or for the larger values of the ratio $M_t^2/(M_1^2-1)$.

Although computations show that there is no signifiant effect of Reynolds number on the amplification of vorticity, there does exist a significant Reynolds-number dependence on the free evolution of vorticity downstream of the shock. For the flow with the higher Reynolds number (figure 9*a*), transverse components decay rather slowly with a slight increase in the streamwise component near the shock wave after the interaction. For the flow with the lower Reynolds number (figure 9*b*), vorticity decays monotonically both upstream and downstream of the shock wave. In order to check if the increase of the streamwise vorticity component behind the shock (figure 9*a*) is caused by poor resolution of the simulation, a coarse grid simulation with $97 \times 48 \times 48$ points was performed. As shown in figure 9(*a*), streamwise vorticity fluctuation predicted by the fine-grid simulation is slightly larger than that of the coarse simulation, which confirms that the increase of the streamwise vorticity component is not a numerical artifact.

In order to identify the dominant mechanisms for the vorticity amplification and clarify the Reynolds-number effect on vorticity evolution, we examined the budget of the transport equation of the vorticity variances $\overline{\omega_\alpha'^2}$,

$$\underbrace{\bar{u}_j \frac{\partial \overline{\omega_\alpha'^2}}{\partial x_j}}_{\text{(I)}} = \underbrace{2\overline{\omega_\alpha' \omega_j'} \bar{s}_{\alpha j}}_{\text{(II)}} + \underbrace{2\overline{\omega_\alpha' \omega_j' s_{\alpha j}'}}_{\text{(III)}} - \underbrace{2\overline{\omega_\alpha'^2} \bar{s}_{jj}}_{\text{(IV)}} - \underbrace{\overline{\omega_\alpha'^2 s_{jj}'}}_{\text{(V)}} + \underbrace{2\epsilon_{\alpha jk} \overline{\omega_\alpha' \rho_{,j} p_{,k}/\rho^2}}_{\text{(VI)}} - \underbrace{(\overline{\omega_\alpha'^2 u_k'})_{,k}}_{\text{(VII)}} + \underbrace{\Phi_\alpha}_{\text{(VIII)}}, \tag{4}$$

where the repeated Greek indices are not summed. Here, $s_{ij} = \frac{1}{2}(u_{i,j} + u_{j,i})$ is a strain rate tensor and Φ_α is the viscous dissipation and transport, given by

$$\Phi_\alpha = 2\epsilon_{\alpha jk} \overline{\omega_\alpha' \left(\frac{1}{\rho} \tau_{kq,q}\right)_{,j}}.$$

The term (I) on the left-hand side of (4) represents the advection by the mean flow. The first and second terms (II, III) on the right-hand side represent vortex stretching by the mean and turbulent strain fields, respectively. The next two terms (IV, V) represent vorticity–compression products. (VI) is the production by the baroclinic torque, (VII) the transport by the turbulent velocity field, and the last term (VIII) is the viscous dissipation and transport.

The balance of the terms in (4) is investigated for the transverse vorticity $\overline{\omega_2'^2}$. Inside the shock wave, the vorticity–compression (IV + V) is the leading term for vorticity amplification. The viscous term (VIII) balances with the vortex stretching (II + III) beyond the shocked region. Baroclinic torque (VI) is less than 1% of the leading terms throughout the domain for all the simulations we performed, including case F where the shock wave is strongly distorted. The effect of turbulent transport (VII) is also found to be negligible. The vorticity–mean compression (IV) is much larger than the

other terms inside the shock. The dominance of the vorticity–mean compression explains the good comparison of the simulation results with the LIA predictions.

The balance of terms in (4) for the streamwise vorticity $\overline{\omega_1'^2}$ is investigated for case A and case C. Inside the shock wave, effects of vortex stretching (II + III) and vorticity–compression (IV + V) tend to cancel, resulting in no appreciable change in the streamwise vorticity. As shown in figures 9(*a*) and 9(*b*), there is a significant difference in the evolution of the streamwise vorticity for flows with different Reynolds numbers. Outside the interaction zone, the dominating terms in (4) are the viscous term (VIII) and the vortex stretching (II + III) – mainly by the turbulent strain field. Through the interaction, turbulent vortex stretching is sufficiently amplified to overtake the viscous dissipation behind the shock wave for the higher Reynolds number flow, resulting in the increase in the streamwise vorticity component behind the shock wave (figure 9*a*). Intensification of the turbulent stretching mechanism for the lower Reynolds number flow is not sufficiently pronounced to overcome the viscous dissipation. This trend can be regarded as the Reynolds-number dependence of low Reynolds number turbulence which is undergoing relaxation from a strained state.

3.5. *Turbulence lengthscale*

Experimental studies (Debieve & Lacharme 1986; Keller & Merzkirch 1990; Honkan & Andreopoulos 1992) have reported that large-scale turbulent motions are enhanced more than small-scale motions as turbulence passes through a shock wave, leading to the overall increase of turbulence lengthscales, especially of Taylor microscales. In order to check whether turbulence lengthscales do indeed increase, we investigated the amplification of the one-dimensional velocity spectra, $E_{11}(\omega)$ and $E_{11}(k_1)$, through the linear analysis. In the following, we consider only the contribution of the vorticity waves to the upstream and downstream velocity fluctuations, since the contribution of the acoustic waves is negligible after a short distance behind the shock (figure 4). Predictions of LIA on the amplification of the spectra depend on the shape of the spectrum,† and the von Kármán spectrum

$$E(k) \sim \frac{(k/k_0)^4}{[1+(k/k_0)^2]^{17/6}}$$

is chosen for the analysis presented here. The amplification ratios for the one-dimensional frequency spectrum and wavenumber spectrum for different shock strengths are shown in figures 10(*a*) and 10(*b*), respectively. The frequency spectrum amplification depends on the choice of the reference frame, but the wavenumber spectrum amplification is independent of the choice. (Figure 10 corresponds to the frame of reference fixed on the mean shock position.) The spectrum amplification ratio is larger for a low-frequency wave, which is consistent with the results of Ribner (1987). Some researchers have interpreted this fact as evidence of turbulence lengthscale increase through the interaction, but this conclusion is incorrect as a change in frequency spectra reflects a change in timescale, not in lengthscale. Higher amplification at the small-frequency part of the spectrum implies that the turbulence timescale increases through the interaction. By considering the mean flow deceleration through the shock and applying Taylor's hypothesis, the frequency spectrum amplification (figure 10*a*) can be converted into wavenumber spectrum amplification, figure 10(*b*) (for details, see Lee *et al.* 1992*b*). The wavenumber spectrum is amplified more at large wavenumbers. A correct interpretation of LIA provides enhanced small scales and for

† Even though the spectrum amplification depends on the spectrum shape, the Taylor microscale ratio across the shock wave is independent of the spectrum shape for isotropic turbulence.

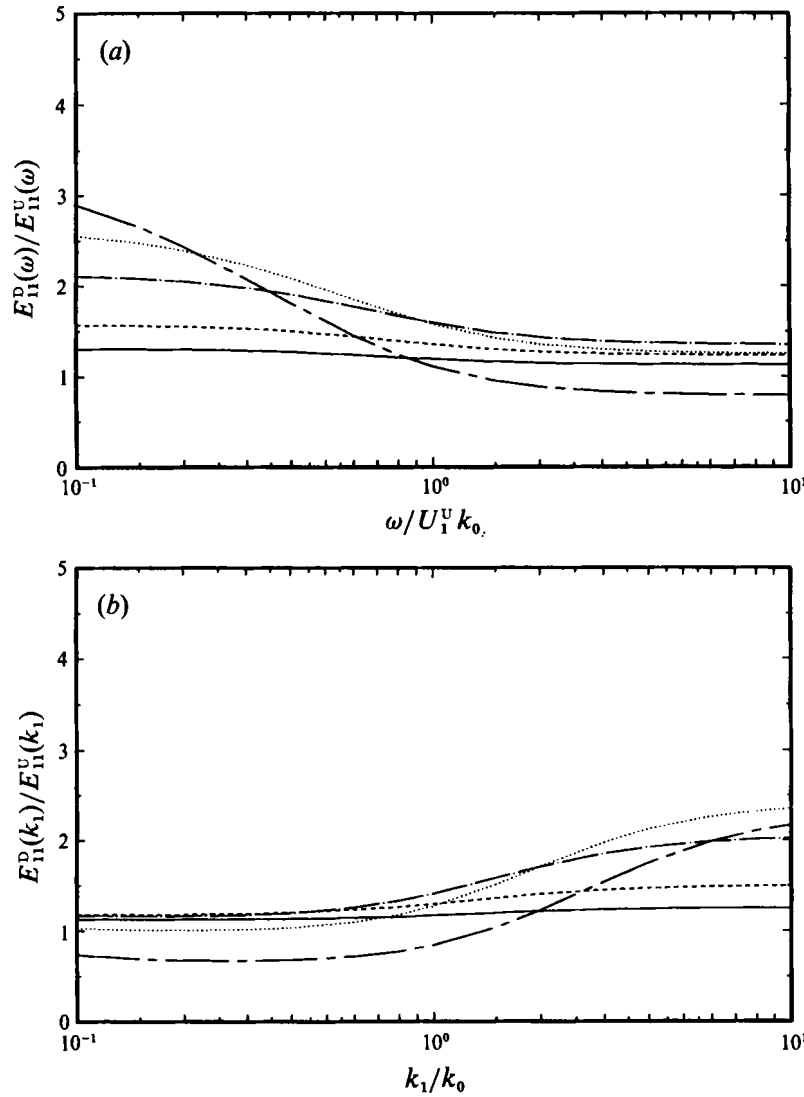

FIGURE 10. Amplification ratio of (*a*) frequency spectrum and (*b*) wavenumber spectrum predicted by LIA: ——, $M_1 = 1.1$; – – –, $M_1 = 1.2$; —·—, $M_1 = 1.5$; · · · · · ·, $M_1 = 2.0$; ——, $M_1 = 5.0$. The superscripts U and D denote the upstream and downstream states respectively.

large M_1 a suppression of the spectrum at small wavenumbers. Larger amplification at large wavenumbers is more pronounced for stronger shock waves. It is, therefore, erroneous to infer an increase in turbulence lengthscale in shock turbulence interaction by appealing to Ribner's analysis (akin to figure 10*a*) as in Keller & Merzkirch (1990). Investigation of the spectrum amplification leads to the conclusion that the turbulence timescale increases through the interaction, while the turbulence lengthscale decreases.

The experimental results by Debieve & Lacharme (1986) are consistent with the present predictions. However, they compared the upstream frequency spectrum to that *on* the shock and concluded an increase in the lengthscale. The spectrum on the shock is contaminated by the intermittency effect due to the unsteady shock front distortion. The characteristic lengthscale of the distortion scales with the upstream turbulence lengthscale (see §4 for details) to yield apparent amplification of the spectrum on the

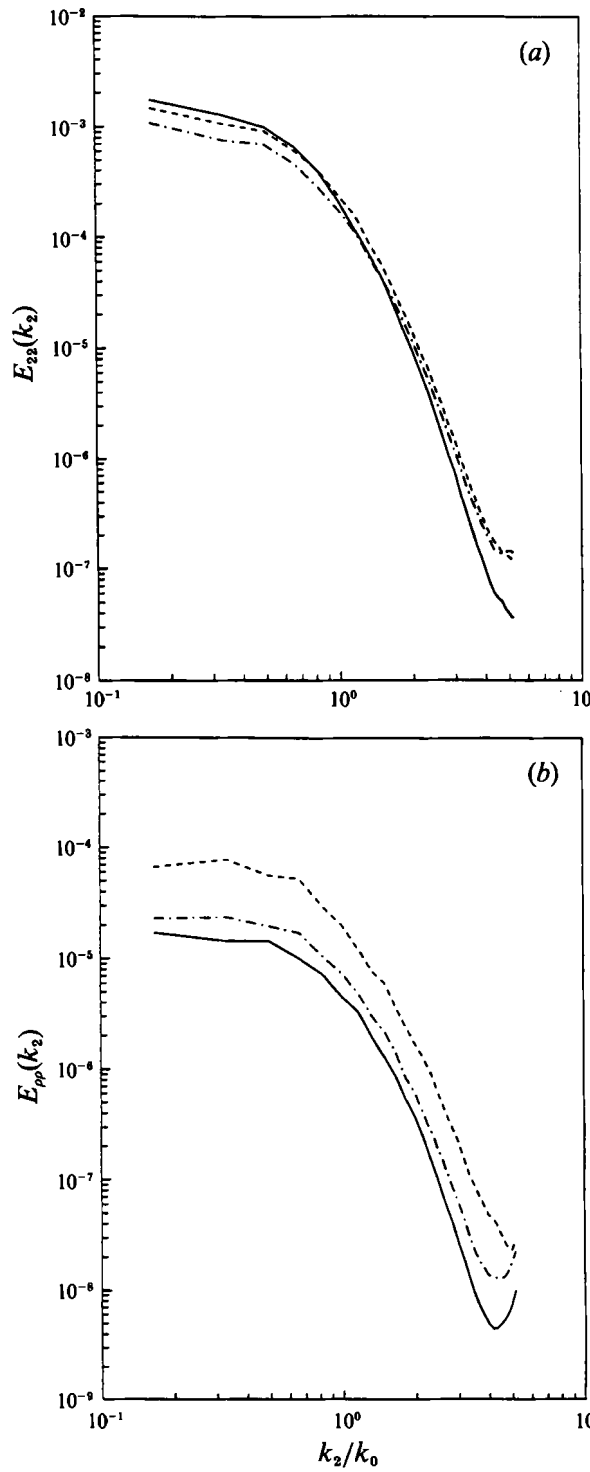

FIGURE 11. Evolution of the energy spectra of (*a*) transverse velocity and (*b*) density fluctuation for case C: ——, upstream ($k_0 x_1 = 15.8$); – – – –, immediate downstream ($k_0 x_1 = 21.9$); —·—, further downstream ($k_0 x_1 = 29.1$).

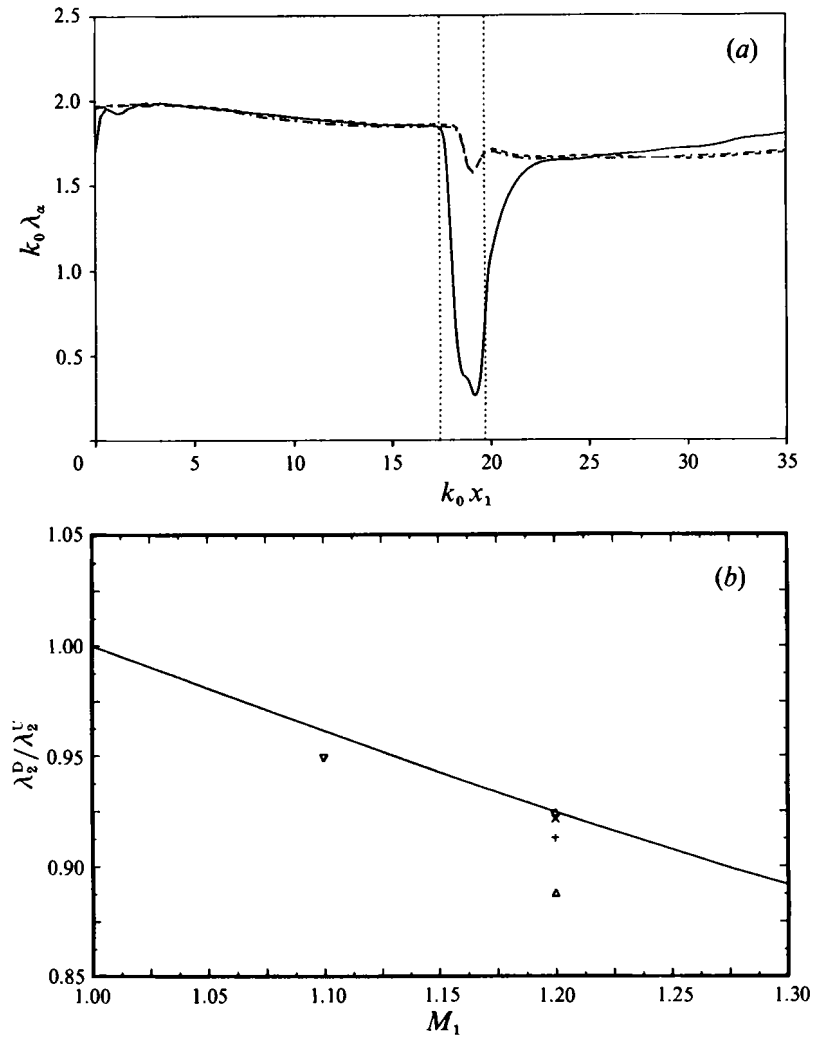

FIGURE 12. (*a*) Evolution of Taylor microscales for case C: ——, λ_1; – – –, λ_2; —·—, λ_3. Vertical lines denote the boundaries of shock intermittency. (*b*) Comparison of Taylor microscale change across the shock wave with LIA prediction: ——, LIA, symbols from DNA; △, case A; +, B; ×, C; ◇, D; ▽, E. The superscripts U and D denote the upstream and downstream states, respectively.

shock at energetic (or large) scales. This enhancement does not necessarily imply the amplification of the turbulent motion of that scale. The upstream *wavenumber* spectrum should be compared with the downstream *wavenumber* spectrum. Proper comparison of wavenumber spectra shows more amplification at small scales than at large scales, leading to an overall scale decrease.

Figures 11(*a*) and 11(*b*) show the evolution of the one-dimensional power spectra of $u_2'(E_{22}(k_2))$ and density ($E_{\rho\rho}(k_2)$), respectively. Across the shock wave, enhancement of the spectrum in figure 11(*a*) can be noticed with more amplification at large wavenumbers. As the flow evolves further downstream of the shock, the spectrum drops over the entire range of wavenumbers. More amplification at large wavenumbers across the shock wave leads to a decrease of the turbulence lengthscales, especially the Taylor microscale. This is shown in figure 12(*a*). Density fluctuations are amplified across the shock wave due to the amplification and generation of acoustic waves

through the interaction. There is no appreciable wavenumber dependence in the amplification of the power spectrum of density fluctuations.

The evolution of the longitudinal Taylor microscales λ_α is plotted in figure 12(*a*). Noticeable reductions of all the microscales are found across the shock wave. The evaluation of the streamwise microscale λ_1 inside the shock wave is significantly contaminated due to the shock front intermittency. Since it is difficult to identify a 'downstream value' of λ_1 due to its rapid evolution behind the shock, figure 12(*b*) compares Taylor microscale reductions only in a transverse direction with LIA predictions. Except for cases with strong upstream turbulence intensity, the simulation results compare favourably with the LIA predictions. As the upstream turbulence intensity increases, the lengthscales decrease more for the same M_1 (compare cases A, B, C and D). In conclusion, direct numerical simulation confirms that turbulence lengthscales do decrease through the shock–turbulence interaction.

3.6. *Thermodynamic properties*

Thermodynamic properties are held uniform in space and constant in time at the inflow boundary, and fluctuations in thermodynamic variables develop as the flow evolves downstream. In figure 13(*a*), we present the evolution of r.m.s. pressure, density, and temperature fluctuations ($p_{\rm rms}$, $\rho_{\rm rms}$, and $T_{\rm rms}$) throughout the field. As the flow passes through the shock wave, all the fluctuations are amplified, followed by a rapid decay. A polytropic exponent $n(x_1)$ relating the pressure and density fluctuations may be defined as

$$n(x_1) = \frac{p_{\rm rms}(x_1)/\bar{p}(x_1)}{\rho_{\rm rms}(x_1)/\bar{\rho}(x_1)},$$

which is equal to γ (1.40 here) for isentropic fluctuations. The polytropic exponents deduced from the simulations stay close to the isentropic value throughout the domain for all the simulations, varying between 1.35 and 1.40. The joint probability density function (JPDF) of pressure and density was computed to investigate if the isentropic relation is also satisfied for instantaneous states. Figure 13(*b*) shows the JPDF of the instantaneous pressure versus instantaneous density scaled with their local mean values, $\bar{p}(x_1)$ and $\bar{\rho}(x_1)$. Clearly the isentropic relations are satisfied between the instantaneous states, even inside the shock wave.

By use of the Gibbs' equation and the equation of state of an ideal gas, the pressure fluctuation can be represented in terms of the fluctuations in density and entropy as

$$p' \approx \left(\frac{\partial p}{\partial \rho}\right)_s \rho' + \left(\frac{\partial p}{\partial s}\right)_\rho s', \tag{5}$$

where s is the entropy. When temperature (or entropy) inhomogeneity in the flow is not significant, or

$$\left|\left(\frac{\partial p}{\partial \rho}\right)_s \rho'\right| \gg \left|\left(\frac{\partial p}{\partial s}\right)_\rho s'\right|,$$

the above relation reduces to the isentropic relation, $p' = \bar{c}^2 \rho'$. This inequality can be translated into the following form (Thompson 1971, p. 144):

$$|u_{i,i}| \gg \left|\frac{(\gamma-1)}{\gamma p}(\epsilon + \kappa \nabla^2 T)\right|. \tag{6}$$

The contribution of the right-hand side of (6) to the dilatation was found to be less than 5% in the present simulations, which verifies the fact that the relations between thermodynamic property fluctuations are nearly isentropic.

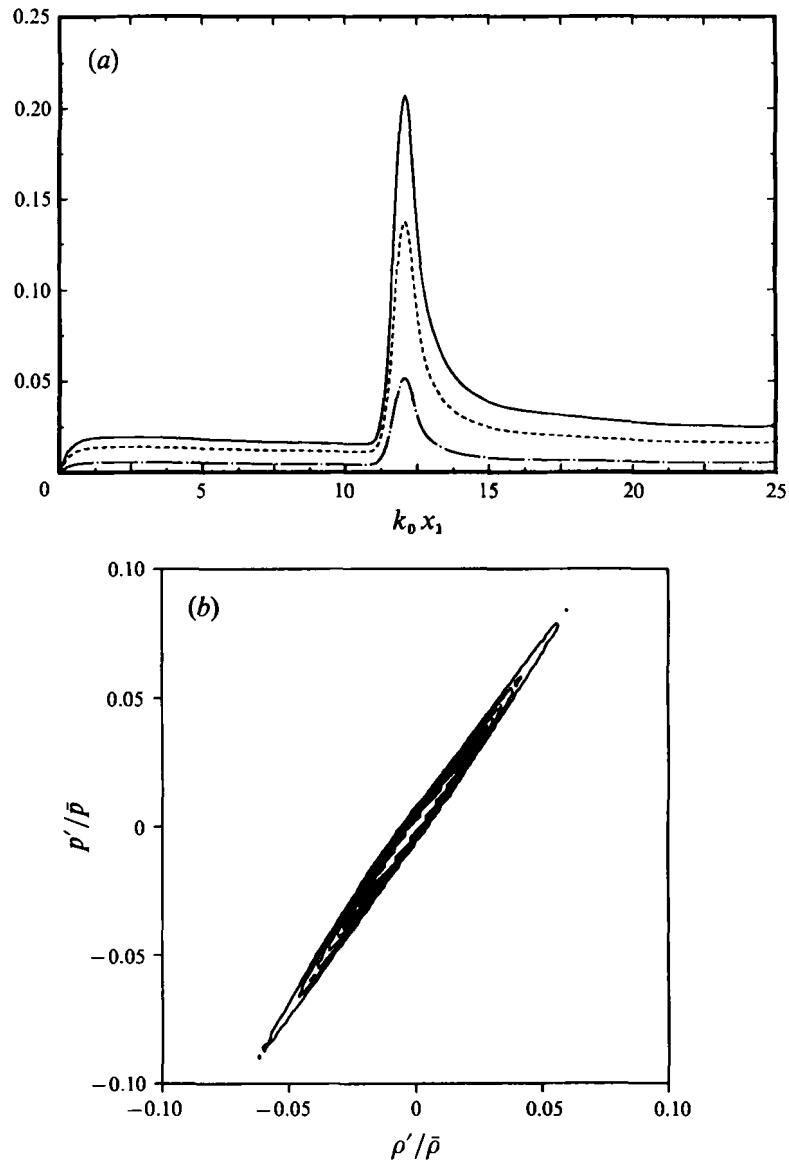

FIGURE 13. (*a*) Evolution of r.m.s. values of thermodynamic properties for case A: ——, $p_{\rm rms}/\bar{p}_{\rm in}$; – – – –, $\rho_{\rm rms}/\bar{\rho}_{\rm in}$; —·—, $T_{\rm rms}/\tilde{T}_{\rm in}$. (*b*) Joint probability density function of scaled instantaneous pressure and density for case C.

This may be contrasted to the case where an appreciable mean temperature gradient exists in the flow and the pressure fluctuation is negligible; the expression (5) with the assumption of negligible stagnation temperature variation leads to the 'strong Reynolds analogy' (Morkovin 1962; Bradshaw 1977)

$$\frac{\rho'}{\bar{\rho}} \approx \frac{-T''}{\tilde{T}} \approx (\gamma-1)\, M_1^2 \frac{u_1''}{\tilde{u}_1}.$$

Note that the correlation coefficient between ρ' and T'' is -1 in the strong Reynolds analogy, while it is $+1$ for isentropic fluctuations. Thus, the widely used Morkovin's

hypothesis which is suitable for compressible turbulent boundary layers is not valid in the present shock/turbulence interaction. Morkovin's hypothesis requires that the density fluctuations be primarily associated with entropy fluctuations. Whereas this condition is presumably met in shear flows, it is not met in the present flow. A similar situation is also encountered in compressible homogeneous turbulence (Blaisdell, Mansour & Reynolds 1990).

In order to identify the mechanisms of amplification and decay of the density fluctuation variance $\overline{\rho'^2}$, the terms in the transport equation for the density fluctuation variance (Taulbee & Van Osdol 1991) were computed:

$$\underbrace{\tilde{u}_1 \frac{\partial \overline{\rho'^2}}{\partial x_1}}_{\text{(I)}} = \underbrace{-2\overline{\rho'^2}\frac{\partial \tilde{u}_1}{\partial x_1}}_{\text{(II)}} \underbrace{-2\overline{\rho' u_1''}\frac{\partial \bar{\rho}}{\partial x_1}}_{\text{(III)}} \underbrace{-2\bar{\rho}\overline{\rho' \frac{\partial u_i''}{\partial x_i}}}_{\text{(IV)}} \underbrace{-\overline{\rho'^2 \frac{\partial u_i''}{\partial x_i}}}_{\text{(V)}} \underbrace{-\frac{\partial \overline{\rho'^2 u_1''}}{\partial x_1}}_{\text{(VI)}}. \tag{7}$$

The convection (I) is balanced by the production due to mean compression (II) and the mean density gradient (III), density–dilatation correlations (IV + V), and turbulent transport (VI). The balance of the terms in (7) is investigated for the density fluctuation variance, $\overline{\rho'^2}$. Across the shock wave, density fluctuation is enhanced mainly by the production due to the mean compression (II) and the mean density gradient (III). Behind the shock wave, however, the evolution of $\overline{\rho'^2}$ is dominated by the turbulent density–dilatation correlation (IV). In summary, density fluctuations are amplified across the shock wave mainly through the mean flow compression, whereas their evolution behind the shock wave is dominated mostly by nonlinear mechanisms.

4. Modification of an instantaneous shock wave

As a shock wave propagates in a turbulent medium, the instantaneous structure of the shock wave is modified. Variations in shock wave strength and shock front distortion due to turbulence are discussed in this section.

The turbulent upstream condition causes the shock wave structure to be non-uniform in the (x_2, x_3)-plane and the shock front to be distorted. Instantaneous density fields at a typical (x_1, x_2)-plane from cases D and F are shown in figures 14(*a*) and 14(*b*): figure 14(*a*) is for weak upstream turbulence ($M_1 = 1.20$, $M_t = 0.057$) and figure 14(*b*) is for a relatively intense turbulence ($M_1 = 1.05$, $M_t = 0.10$). The overlaid contour lines near the centre of the figures are isocompression (constant value of $u_{i,i}$) lines. Figure 14(*a*) shows a clear shock front across which the increase in density occurs, while for the more intense upstream turbulence (figure 14*b*) the shape of the shock front is more distorted. The variation in the transverse directions of the peak compression inside the shock wave, or the shock strength variation, becomes stronger for the more intense upstream turbulence. The variation in the visual thickness of the shock wave is also larger for the stronger upstream turbulence. Low-density regions are often found behind the mean shock position for flows with $M_t^2 > a(M_1^2 - 1)$ ($a \approx 0.1$).

Figures 15(*a*) and 15(*b*) show the profiles of dilatation along different mean flow streamlines from an instantaneous snapshot of the flow for cases D and F, respectively. The strength of the shock wave (or the peak compression in the shock) varies widely from one streamline to another. Strong compression tends to occur in regions where the shock wave is pushed downstream, and weak compression tends to occur in regions where the shock wave is pulled upstream. For the case of intense upstream turbulence (case F), the structure of the shock wave is significantly modified: multiple peaks in

(a)

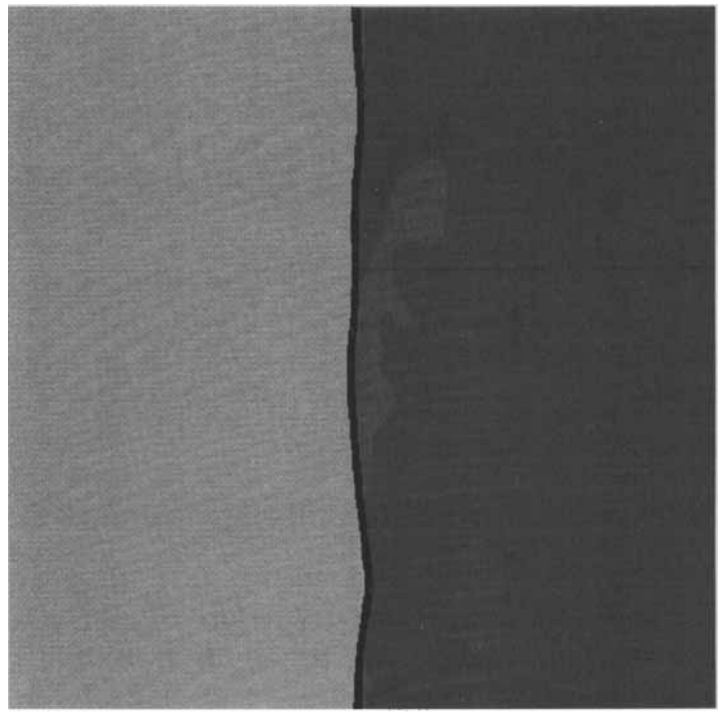

(b)

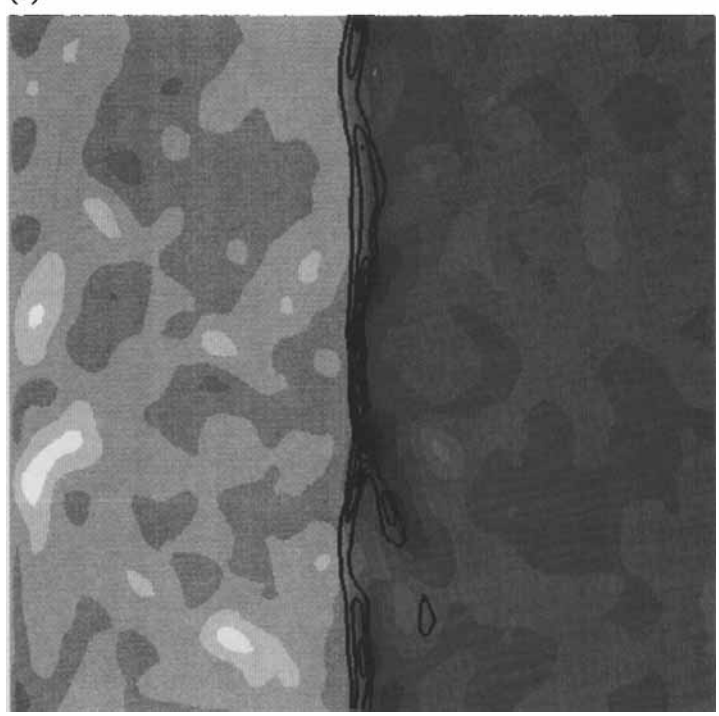

FIGURE 14. Instantaneous density field in a typical (x_1, x_2)-plane for (*a*) case D and (*b*) case F. A region of higher density is denoted by a darker shading. The grey level varies from 0.95 to 1.45 with an increment of 0.05 in case D, and from 0.96 to 1.15 with an increment of 0.01 in case F. The overlaid thick lines near the centres of the figures are isocompression lines.

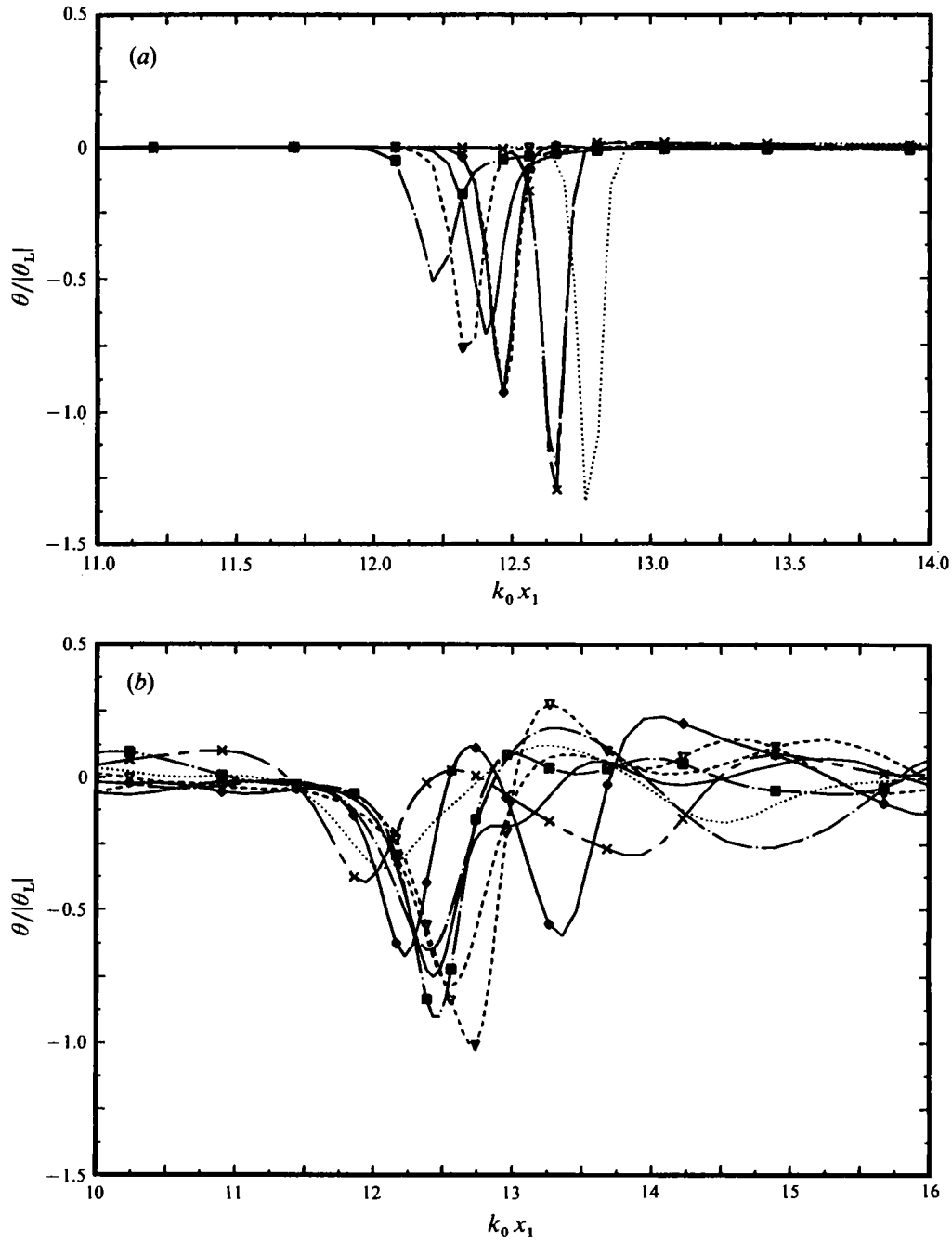

FIGURE 15. Profiles of instantaneous dilatation along the mean streamlines for (*a*) case D and (*b*) case F. θ_L is the peak compressive strain rate in the laminar shock wave at the same upstream Mach number.

compression along streamlines are noticeable. Each compression peak has a strength comparable to the mean shock wave. Sometimes, a shock wave is replaced by a series of compression waves.

The peak compression $\theta_{\min}(x_2, x_3, t)$ inside the shock wave along the mean streamline may be used as a measure of the shock wave strength. The peak value is

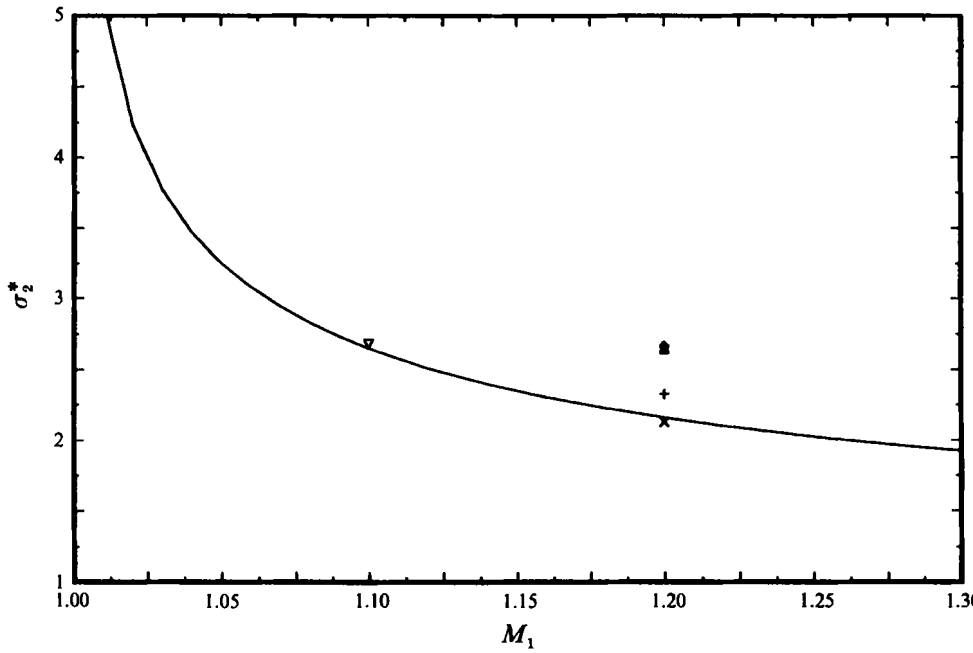

FIGURE 16. Comparison of scaled r.m.s. shock front inclination angles, $\sigma_2^* = \sigma_2(\tilde{u}_1/u_{\rm rms})^{\rm U}$, with LIA predictions: ——, LIA; symbols from DNS: △, case A; +, B; ×, C; ◇, D; ▽, E.

taken along the x_1-direction for each x_2 and x_3. The average peak compression is found to be weaker than the peak compression $\theta_{\rm L}$ of the laminar shock wave by about 10%. The peak compression varies widely across the transverse plane, which is reflected in the large value of the ratio of the r.m.s. and the mean values of the peak compression, $(\theta_{\rm min})_{\rm rms}/|\overline{\theta_{\rm min}}| = 0.42$.

The probability density function (PDF) of the peak compression inside the shock wave shows that the probability of large compression zones is higher than the Gaussian distribution by several orders of magnitude. This trend is more significant for the stronger upstream turbulence, which is confirmed by the skewness (S) and flatness (F) values of the PDF, $S = -0.81, F = 4.03$ for case C and $S = -1.46, F = 6.49$ for case F, respectively.

The statistics of shock front distortion from the simulations are compared with those from the linear analysis. The definition of the shock wave front in the simulated field, however, is not trivial, because in the numerical simulations the shock wave spans over several grid points, $\delta_{\rm s}^{\rm L}/(\Delta x_1)_{\rm min} = 2 \sim 3$. The pressure half-rise point was chosen to be the shock front position, $\xi(x_2, x_3, t)$; that is,

$$\xi(x_2, x_3, t) = \{\xi \,|\, p(\xi, x_2, x_3, t) = \tfrac{1}{2}(p_{\rm L}^{\rm U} + p_{\rm L}^{\rm D})\},$$

where $p_{\rm L}$ denotes the pressure in the laminar shock wave with the same M_1 and the superscripts U and D denote the upstream and downstream states, respectively. This designator is very well-defined and remains relatively noise-free for the cases with weak upstream turbulence. In order to check the sensitivity of the shock front statistics to the special choice of the designator, statistics of the shock wave distortion based on the pressure half-rise point were compared with those based on the density half-rise point. The differences were always less than 1% of the predicted r.m.s. values. Figure 16 shows the scaled r.m.s. shock front inclination angle in the x_2-direction, $\sigma_2 = \partial\xi/\partial x_2$. LIA predicts the r.m.s. shock front inclination angle to be independent of the upstream

energy spectrum shape, and that the inclination angle is proportional to the upstream turbulence intensity. The statistics from the simulation are in fair agreement with the LIA predictions. As the fluctuation Mach number of the simulation increases, the simulation results deviate further from the linear prediction.

LIA predicts that the spanwise wavelength of the shock front movement is the same as that of the upstream turbulence and that fluctuating shock front speed scales with the upstream turbulence velocity (for more details, see Lee *et al.* 1992*b*).

5. Summary and discussion

The interaction of isotropic turbulence with a shock wave has been investigated by means of direct numerical simulations. The results have been compared with the predictions of the linear theory.

The simulations show that the diagonal components of the Reynolds stress tensor, $R_{\alpha\alpha}$ are enhanced across the shock wave. The amplification is larger for stronger shock waves within the range of Mach numbers in the simulation, $1.05 \leqslant M_1 \leqslant 1.20$. The simulations show a rapid increase followed by a decrease of R_{11} downstream of the shock wave. Linear analysis, on the other hand, predicts that R_{11} monotonically decays from its post-shock value to the far-field value. The budget of the TKE transport equation revealed that rapid evolution of TKE is caused mainly by the redistribution of TKE (through the pressure-transport term) in the streamwise direction as the turbulence relaxes from the compression.

The simulations show that transverse vorticity components are amplified and that the streamwise component is not influenced by the interaction. The amplification is larger for stronger shock waves. The amplification of transverse vorticity components predicted by the simulations is in excellent agreement with those of the linear analysis for $M_t^2 < a(M_1^2-1)$ with $a \approx 0.1$. Examination of the budget of $\overline{\omega_\alpha'^2}$ revealed that the vorticity–mean compression $\overline{\omega_\alpha'^2 s_{jj}}$ is the main contributor to the transverse vorticity amplification during the interaction.

The energy spectrum is amplified more at large wavenumbers, leading to the decrease of turbulence lengthscales through the interaction. This is consistent with the prediction of the linear theory: amplification is larger for large wavenumbers in the wavenumber spectrum, while it may be larger for small frequencies in the frequency spectrum.

Thermodynamic property fluctuations are amplified significantly across the shock wave. The relations between scaled r.m.s. property fluctuations are very close to isentropic, at least for turbulence passing through a weak shock wave with $M_1 \leqslant 1.20$. Isentropic relations are satisfied even between the instantaneous fluctuations throughout the flow field including the shock wave.

Owing to the non-uniformity of the upstream turbulence, the shock wave has a time-dependent distorted front and a non-uniform thickness in the transverse directions. For the simulations with $M_t^2 < a(M_1^2-1)$, shock waves have well-defined fronts with a single compression peak along each mean streamline. Shock front distortions are found to be proportional to the upstream turbulence intensities. For a simulation with $M_t^2 > a(M_1^2-1)$, shock waves no longer have well-defined fronts in the transverse directions. Low-density regions are often found behind the mean shock position, and shock wave thickness varies quite widely in transverse directions. Along the streamwise direction, multiple compression peaks are found inside the shock wave.

Direct numerical simulations reported in this paper were limited to interactions of weak shock waves with turbulence at low Reynolds numbers due to resolution

requirements of shock waves and turbulence (for details, see Lee *et al.* 1992*b*). For a strong shock wave, it is impractical to resolve a shock structure not only because the required cost of resolving the shock wave is prohibitive, but also because the Navier–Stokes equations are not valid inside a shock wave for $M_1 > 2.0$. Therefore, numerical simulation of a strong shock wave interacting with turbulence requires a method of treating the shock wave as a discontinuity without loss of numerical accuracy elsewhere. Various methods including shock capturing, shock fitting and filtering schemes are under consideration. The methods of treating the shock wave can be validated by comparing the results with those from DNS where the shock wave is directly resolved.

Direct numerical simulation is impractical for calculations involving high Reynolds number turbulence and strong shock waves. For such cases one must resort to the large-eddy simulation technique where the large-scale motions are resolved and the effects of the unresolved turbulence on the large-scale field are parametrized by subgrid-scale models.

Interaction of isotropic turbulence with a shock wave is only an element of the complex interaction between a shock and a turbulent boundary layer. To fully understand the mechanisms of the interaction, further research is required to investigate the effects of wall presence and mean shear.

The authors would like to acknowledge the financial support from the Air Force Office of Scientific Research under Grant No. 88-NA-322 with Dr Leonidas Sakell as the technical monitor. The use of the computer facilities of NAS and NASA-Ames research center is also greatly appreciated.

REFERENCES

ANDREOPOULOS, J. & MUCK, K.-C. 1987 Some new aspects of the shock-wave boundary-layer interaction in compression ramp corner. *J. Fluid Mech.* **180**, 405–428.

ANYIWO, J. C. & BUSHNELL, D. M. 1982 Turbulence amplification in shock-wave boundary-layer interaction. *AIAA J.* **20**, 893–899.

BLAISDELL, G. A., MANSOUR, N. N. & REYNOLDS, W. C. 1990 Numerical simulations of compressible homogeneous turbulence. *Rep.* TF-50. Department of Mechanical Engineering, Stanford University, CA.

BRADSHAW, P. 1977 Compressible turbulence shear layers. *Ann. Rev. Fluid Mech.* **9**, 33–54.

BUELL, J. C. & HUERRE, P. 1988 Inflow/outflow boundary conditions and global dynamics of spatial mixing layers. *Center for Turbulence Research Proc. Summer Program 1988.* Stanford/NASA Ames.

CHANG, C.-T. 1957 Interaction of a plane shock and oblique plane disturbances with special reference to entropy waves. *J. Aero. Sci.* **24**, 675–682.

COLEMAN, G. N. & MANSOUR, N. N. 1991 Simulation and modeling of homogeneous compressible turbulence under isotropic mean compression. *Proc. Eighth Symp. on Turbulent Shear Flows, Munich* (ed. F. Durst, R. Friedrich, B. E. Launder, F. W. Schmidt, U. Schumann & J. H. Whitelaw). Springer.

DEBIEVE, F.-R., GOUIN, H. & GAVIGLIO, J. 1982 Momentum and temperature fluxes in a shock wave-turbulence interaction. In *Structure of Turbulence in Heat and Mass Transfer* (ed. Z. P. Zarić). Hemisphere.

DEBIEVE, J. F. & LACHARME, J. P. 1986 A shock-wave/free turbulence interaction. In *Turbulent Shear Layer/Shock Wave Interactions* (ed. J. Délery). Springer.

DOLLING, D. S. & OR, C. T. 1985 Unsteadiness of the shock wave structure in attached and separated compression ramp flows. *Exp. Fluids* **3**, 24–32.

FAVRE, A. 1965 Équations des gaz turbulents compressibles I. *J. Méc.* **4**, 361–390.

FAVRE, A., KOVASZNAY, L. S. G., DUMAS, R., GAVIGLIO, J. & COANTIC, M. 1976 *La Turbulence en Mécanique des Fluides*. Gauthier-Villars.

GILES, M. B. 1990 Nonreflecting boundary conditions for Euler equation calculations. *AIAA J.* **28**, 2050–2058.

HESSELINK, L. & STURTEVANT, B. 1988 Propagation of weak shocks through a random medium. *J. Fluid Mech.* **196**, 513–553.

HINZE, J. O. 1975 *Turbulence*, 2nd Edn. McGraw-Hill.

HONKAN, A. & ANDREOPOULOS, J. 1992 Rapid compression of grid-generated turbulence by a moving shock wave. *Phys. Fluids* A **4**, 2562–2572.

JACQUIN, L., BLIN, E. & GEFFROY, P. 1991 Experiments on free turbulence/shock wave interaction. *Proc. Eighth Symp. on Turbulent Shear Flows, Munich* (ed. F. Durst, R. Friedrich, B. E. Launder, F. W. Schmidt, U. Schumann & J. H. Whitelaw). Springer.

KELLER, J. & MERZKIRCH, W. 1990 Interaction of a normal shock wave with a compressible turbulent flow. *Exp. Fluids* **8**, 241–248.

KERREBROCK, J. L. 1956 The interaction of flow discontinuities with small disturbances in a compressible fluid. PhD thesis, California Institute of Technology.

KOVÁSZNAY, L. S. G. 1953 Turbulence in supersonic flow. *J. Aero. Sci.* **20**, 657–682.

LEE, S., LELE, S. K. & MOIN, P. 1991*a* Direct numerical simulation and analysis of shock turbulence interaction. *AIAA Paper* 91-0523.

LEE, S., LELE, S. K. & MOIN, P. 1991*b* Eddy-shocklets in decaying compressible turbulence. *Phys. Fluids* A **3**, 657–664.

LEE, S., LELE, S. K. & MOIN, P. 1992*a* Simulation of spatially evolving compressible turbulence and the applicability of Taylor's hypothesis. *Phys. Fluids* A **4**, 1521–1530.

LEE, S., MOIN, P. & LELE, S. K. 1992*b* Interaction of isotropic turbulence with a shock wave. *Rep.* TF-52. Department of Mechanical Engineering, Stanford University, Stanford, CA.

LELE, S. K. 1992*a* Compact finite difference schemes with spectral-like resolution. *J. Comput. Phys.* **103**, 16–42.

LELE, S. K. 1992*b* Shock-jump relations in a turbulent flow. *Phys. Fluids* A **4**, 2900–2905.

LIGHTHILL, M. J. 1953 On the energy scattered from the interaction of turbulence with sound or shock waves. *Proc. Camb. Phil. Soc.* **49**, 531–551.

LUMPKIN, F. E. 1990 Development and evaluation of continuum models for translational-rotational nonequilibrium. PhD thesis, Stanford University.

MCKENZIE, J. F. & WESTPHAL, K. O. 1968 Interaction of linear waves with oblique shock waves. *Phys. Fluids* **11**, 2350–2362.

MOORE, F. K. 1953 Unsteady oblique interaction of a shock wave with a plane disturbances. *NACA TN*-2879. Also *NACA Rep.* 1165.

MORKOVIN, M. V. 1962 Effects of compressibility on turbulent flows. In *Mechanique de la Turbulence*, CNRS.

RIBNER, H. S. 1953 Convection of a pattern of vorticity through a shock wave. *NACA TN*-2864. Also *NACA Rep.* 1164.

RIBNER, H. S. 1954 Shock-turbulence interaction and the generation of noise. *NACA TN*-3255. Also *NACA Rep.* 1233.

RIBNER, H. S. 1969 Acoustic energy flux from shock-turbulence interaction. *J. Fluid Mech.* **35**, 299–310.

RIBNER, H. S. 1987 Spectra of noise and amplified turbulence emanating from shock-turbulence interaction. *AIAA J.* **25**, 436–442.

ROTMAN, D. 1991 Shock wave effects on a turbulent flow. *Phys. Fluids* A **3**, 1792–1806.

SARKAR, S., ERLEBACHER, G., HUSSAINI, M. Y. & KREISS, H. O. 1991 The analysis and modeling of dilatational terms in compressible turbulence. *J. Fluid Mech.* **227**, 473–493.

SHERMAN, F. S. 1955 A low-density wind-tunnel study of shock-wave structure and relaxation phenomena in gases. *NACA TN*-3298.

SMITS, A. J. & MUCK, K.-C. 1987 Experimental study of three shock wave/turbulent boundary layer interactions. *J. Fluid Mech.* **182**, 294–314.

TAULBEE, D. & OSDOL, VAN J. 1991 Modeling turbulent compressible flows: the mass fluctuating velocity and squared density. *AIAA Paper* 91-0524.

TAVOULARIS, S., BENNETT, J. C. & CORRSIN, S. 1978 Velocity-derivative skewness in small Reynolds number, nearly isotropic turbulence. *J. Fluid Mech.* **176**, 33–66.

THOMPSON, K. W. 1987 Time dependent boundary conditions for hyperbolic systems. *J. Comput. Phys.* **68**, 1–24.

THOMPSON, P. A. 1971 *Compressible-Fluid Dynamics*. McGraw-Hill.

TREFETHEN, L. N. 1982 Group velocity in finite difference schemes. *SIAM Rev.* **24**, 113–136.

VICHNEVETSKY, R. 1986 Invariance theorems concerning reflection at numerical boundaries. *J. Comput. Phys.* **63**, 268–282.

WRAY, A. A. 1986 Very low storage time-advancement schemes. *Internal Rep.* NASA-Ames Research Center, Moffett Field, CA.